infected murine neuroblastoma cells produce protease-resistant prion proteins, J. Virol. 62 (1988) 1558–1564.
[15] M.R. Scott, R. Kohler, D. Foster, S.B. Prusiner, Chimeric prion protein expression in cultured cells and transgenic mice, Protein Sci. 1 (1992) 986–997.
[16] T.A. Schroer, M.P. Sheetz, Role of kinesin and kinesin-associated proteins in organelle transport, in: F.D. Warner, J.R. McIntosh (Eds.), Cell Movement, Alan R. Liss, New York, 1989, pp. 295–306.
[17] A.C. Magalhaes, J.A. Silva, K.S. Lee, V.R. Martins, V.F. Prado, S.S.G. Ferguson, M.V. Gomez, R.R. Brentani, M.A.M. Prado, Endocytic intermediates involved with the intracellular trafficking of a fluorescent cellular prion protein, J. Biol. Chem. 277 (2002) 33311–33318.
[18] R.J. Kascsak, R. Rubenstein, P.A. Merz, M. Tonna-DeMasi, R. Fersko, R.I. Carp, H.M. Wisniewski, H. Diringer, Mouse polyclonal and monoclonal antibody to scrapie-associated fibril proteins, J. Virol. 61 (1987) 3688–3693.
[19] M. Rogers, D. Serban, T. Gyuris, M. Scott, T. Torchia, S.B. Prusiner, Epitope mapping of the Syrian hamster prion protein utilizing chimeric and mutant genes in a vaccinia virus expression system, J. Immunol. 147 (1991) 3568–3574.
[20] K.-M. Pan, N. Stahl, S.B. Prusiner, Purification and properties of the cellular prion protein from Syrian hamster brain, Protein Sci. 1 (1992) 1343–1352.
[21] S.-L. Shyng, J.E. Heuser, D.A. Harris, A glycolipid-anchored prion protein is endocytosed via clathrin-coated pits, J. Cell Biol. 125 (1994) 1239–1250.
[22] S.-L. Shyng, K.L. Moulder, A. Lesko, D.A. Harris, The N-terminal domain of a glycolipid-anchored prion protein is essential for its endocytosis via clathrin-coated pits, J. Biol. Chem. 270 (1995) 14793–14800.
[23] M. Nunziante, S. Gilch, H.M. Schatzl, Essential role of the prion protein N terminus in subcellular trafficking and half-life of cellular prion protein, J. Biol. Chem. 278 (2003) 3726–3734.
[24] A.B. Bowman, A. Kamal, B.W. Ritchings, A.V. Philp, M. McGrail, J.G. Gindhart, L.S. Goldstein, Kinesin-dependent axonal transport is mediated by the sunday driver (SYD) protein, Cell 103 (2000) 583–594.
[25] K.J. Verhey, D. Meyer, R. Deehan, J. Blenis, B.J. Schnapp, T.A. Rapoport, B. Margolis, Cargo of kinesin identified as JIP scaffolding proteins and associated signaling molecules, J. Cell Biol. 152 (2001) 959–970.
[26] M. Schliwa, G. Woehlke, Molecular motors, Nature 422 (2003) 759–765.
[27] R.S. Hegde, J.A. Mastrianni, M.R. Scott, K.A. DeFea, P. Tremblay, M. Torchia, S.J. DeArmond, S.B. Prusiner, V.R. Lingappa, A transmembrane form of the prion protein in neurodegenerative disease, Science 279 (1998) 827–834.
[28] D.R. Brown, K. Qin, J.W. Herms, A. Madlung, J. Manson, R. Strome, P.E. Fraser, T. Kruck, A. von Bohlen, W. Schulz-Schaeffer, A. Giese, D. Westaway, H. Kretzschmar, The cellular prion protein binds copper in vivo, Nature 390 (1997) 684–687.
[29] P.C. Pauly, D.A. Harris, Copper stimulates endocytosis of the prion protein, J. Biol. Chem. 273 (1998) 33107–33110.
[30] M.L. Kramer, H.D. Kratzin, B. Schmidt, A. Romer, O. Windl, S. Liemann, S. Hornemann, H. Kretzschmar, Prion protein binds copper within the physiological concentration range, J. Biol. Chem. 276 (2001) 16711–16719.
[31] W.S. Perera, N.M. Hooper, Ablation of the metal ion-induced endocytosis of the prion protein by disease-associated mutation of the octarepeat region, Curr. Biol. 11 (2001) 519–523.
[32] A.P. Garnett, J.H. Viles, Copper binding to the octarepeats of the prion protein. Affinity, specificity, folding, and cooperativity: insights from circular dichroism, J. Biol. Chem. 278 (2003) 6795–6802.
[33] N. Naslavsky, R. Stein, A. Yanai, G. Friedlander, A. Taraboulos, Characterization of detergent-insoluble complexes containing the cellular prion protein and its scrapie isoform, J. Biol. Chem. 272 (1997) 6324–6331.

Non-glycosylphosphatidylinositol (GPI)-anchored recombinant prion protein with dominant-negative mutation inhibits PrP^{Sc} replication *in vitro*

Hitaru Kishida[1,2], Yuji Sakasegawa[1,3], Kota Watanabe[1,3], Yoshio Yamakawa[4], Masahiro Nishijima[4], Yoshiyuki Kuroiwa[2], Naomi S. Hachiya[1,3] and Kiyotoshi Kaneko[1,3]

1. Department of Cortical Function Disorders, National Institute of Neuroscience, National Center of Neurology and Psychiatry, Kodaira, Tokyo, Japan
2. Department of Neurology, Yokohama City University, Yokohama, Japan
3. Core Research for Evolutional Science and Technology (CREST), Japan Science and Technology Corporation, Kawagoe, Saitama, Japan
4. Department of Biochemistry and Cell Biology, National Institute of Infectious Diseases, Tokyo, Japan

Key Words: recombinant prion protein (rPrP), dominant negatives, Q218K, quinacrine, glycosylphosphatidylinositol (GPI)-anchor, lipid rafts, Creutzfeldt-Jakob disease (CJD)

Abbreviations: PrP = prion protein, GPI = glycosylphosphatidylinositol, CJD = Creutzfeldt-Jakob disease, rPrP = recombinant prion protein, EC_{50} = 50% effective concentration, EC_{99} = 99% effective concentration, PrP^{C} = host-encoded cellular prion protein, PrP^{Sc} = abnormal protease-resistant pathogenic prion protein, TSE = transmissible spongiform encephalopathy, BSE = bovine spongiform encephalopathy, IPTG = Isopropyl-β-D-thiogalactopyranoside, β-ME = β-mercaptoethanol, PMSF = Phenylmethylsulfonyl fluoride, PBS = phosphate buffer saline, PK = proteinase K, WST-8 = 2- (2-methoxy-4-nitrophenyl)- 3- (4-nitrophenyl)- 5- (2,4-disulfophenyl)- 2H- tetrazolium, monosodium salt, SPR = surface plasmon resonance, PIPLC = phosphatidyl-inositol specific phospholipase C

Abstract

Dominant-negative mouse prion protein (PrP) with a lysine mutation at codon 218 (Q218K) is known to inhibit prion replication. In order to gain further mechanistic insight into such dominant negative inhibition, non-glycosylphosphatidylinositol (GPI)-anchored recombinant PrP with Q218K (rPrP-Q218K) was investigated. When applied into scrapie-infected mouse neuroblastoma (ScN2a) cells, rPrP-Q218K but not wild-type rPrP (rPrP-WT) exclusively inhibited abnormal protease-resistant pathogenic isoform (PrP^{Sc}) replication without reducing the viability of the cells. It was even more efficient than quinacrine, which has already been prescribed for sporadic Creutzfeldt-Jakob disease (CJD) patients; 50% effective concentration (EC_{50}) = 0.20 μM, 99% effective concentration (EC_{99}) = 0.86 μM vs. EC_{50} = 0.45 μM, EC_{99} = 1.5 μM. Besides, no apparent cell damage was observed at the concentration of up to 4.3 μM (100 μg/ml). In combination treatment with 0.43 μM (10 μg/ml) of rPrP-Q218K, EC_{99} of quinacrine was decreased from 1.5 μM to 0.5 μM, and the cell viability was recovered from 50% to over 90% as inversely proportional to the concentration of quinacrine. Such combination could alleviate the side effects of quinacrine by reducing its effective concentration without changing or even acceleration the inhibition efficacy. Since homogeneous, high-quality rPrPs could be easily prepared from Escherichia coli in large quantities, rPrP-Q218K is a good candidate for a prion replication antagonist.

Correspondence: Dr. Kiyotoshi Kaneko, MD, Department of Cortical Function Disorders, National Institute of Neuroscience, National Center of Neurology and Psychiatry, 4-1-1 Ogawahigashi Kodaira, Tokyo 187-8502, Japan
Tel: 81-42-346-1718 Fax: 81-42-346-1748 E-mail: kaneko@ncnp.go.jp

Submitted: July 14, 2003 Revision Accepted: October 22, 2003

DOI: 10.1080/13506120410001689634

Introduction

Human prion disease or transmissible spongiform encephalopathy (TSE), such as sporadic Creutzfeldt-Jakob disease (CJD) and variant CJD transmitted from bovine spongiform encephalopathy (BSE) constitutes a group of invariably fatal neurodegenerative disorders[1,2]. Prion protein (PrP) consists of two isoforms, one is a host-encoded cellular isoform (PrP^{C}) and the other is an abnormal protease-resistant pathogenic isoform (PrP^{Sc}). The latter is a causative agent of prion disease. PrP^{Sc} stimulates the conversion of PrP^{C} into nascent PrP^{Sc}, and the accumulation of PrP^{Sc} leads to the central nervous system (CNS) dysfunction and neuronal degeneration[3].

A human polymorphic lysine variant at codon 219 (E219K) in the Japanese population, known to render humans resistant to sporadic CJD[4,5], acts as a dominant negative in scrapie-infected mouse neuroblastoma (ScN2a) culture cells after gene transfection[6,7] and transgenic mice expressing lysine at codon 218 in mouse PrP (mouse Q218K, which corresponds to human E219K)[8]. Of note, such a genetic population with E219K and the transgenic mice with Q218K complete their life span with no apparent phenotypic abnormality[5,8].

We now demonstrate that administration of non-glycosylphosphatidylinositol (GPI)-anchored recombinant PrP (rPrP) with Q218K mutation (rPrP-Q218K) but not wild-type rPrP (rPrP-WT) exclusively inhibited the PrP^{Sc} formation in ScN2a cells, even more efficiently than quinacrine, which has already been prescribed for CJD patients, and no apparent cell damage was observed up to 5-fold higher concentrations of a 99% effective concentration (EC_{99}). When combined, rPrP-Q218K efficiently reduced the effective dosage of quinacrine, and thus rendered ScN2a culture cells more viable. Such a combination could alleviate the side effects of quinacrine by reducing its effective concentration without changing or even accelerating the inhibition efficacy. Since homogeneous, high-quality rPrP could be easily prepared from *Escherichia coli* in large quantities, rPrP-Q218K might be a good candidate as a prion replication antagonist.

Materials and methods

Expression plasmid construction

The gene, mouse (Mo) PrP(23-230), coding for residues 23-230 of mouse PrP was PCR-amplified from mouse brain cDNA using the oligonucleotide primers (5′-GGAATTCACCATGAAAAAGCGGCCAAAGCCTGGAGGG-3′ and 5′-CCGCTCGAGTCAGGATCTTCTCCCGTCGTAATAGGC-3′) and cloned via *EcoRI* and *XhoI* sites into the plasmid pBluescript II SK(+) (Stratagene, La Jolla, CA). The genes for 3F4-tagged MoPrP (MHM2PrP) were also cloned using PCR amplification from pSPOX-MHM2PrP[9,10] as above. The Q218K mutation was generated by PCR-directed mutagenesis using primers (5′-ATGTGCGTCACCCAGTACAAAAAGGAGTCC-3′ and 5′-ATAGGCCTGGGACTCCTTTTTGTACTGGGT-3′). The DNA fragments were cloned into a modified pET-11a (Invitrogen, Carlsbad, CA), pEY2, of which *EcoRI* and *XhoI* sites were introduced as multi-cloning sites, via *EcoRI* and *XhoI* sites.

Purification of recombinant prion proteins (rPrPs)

The rPrPs were expressed as inclusion bodies in the *E. coli* BL21(DE3) (Stratagene) in the presence of 0.1 mM Isopropyl-β-D-thiogalactopyranoside (IPTG). The inclusion bodies were collected from sonicated lysates by centrifugation at 27,000 × g for 10 min, washed three times in Buffer A (2 M urea, 50 mM Tris-HCl, pH 7.5, 150 mM NaCl, 2 mM β-mercaptoethanol (β-ME), 0.5 mM Phenylmethylsulfonyl fluoride (PMSF)), and solubilized in Buffer B (8 M urea, 25 mM Tris-HCl, pH 7.5, 2 mM β-ME, 0.5 mM PMSF). After centrifugation (200,000 × g, 30 min), the supernatant was applied to a CM-Sepharose column (Amersham Bioscience, Piscataway, NJ), washed with Buffer B containing 100 mM NaCl and eluted with Buffer B containing 150 mM NaCl. The eluate containing rPrP was applied to an Ni-NTA agarose column (Qiagen, Valencia, CA), washed with Buffer B containing 5 mM imidazole and eluted with Buffer B containing 200 mM imidazole. The eluate was diluted 10-fold 1 M arginine-HCl, pH 8.0, 1 mM reduced glutathione, 0.8 mM oxidized glutathione and incubated at 4°C overnight. After incubation at 37°C for 10 min, the refolded recombinant proteins were concentrated and buffer-changed into phosphate buffer saline (PBS) by Ultrafree-15 10K NMWL (Millipore, Billerica, MA). Concentrations of rPrP were calculated by the absorbance at 280 nm with specific absorbance unit ($A_{280nm,\ 1mg/mL,\ 1cm}$) of 2.70.

Inhibition assay of PrP^{Sc} accumulation in ScN2a cells

ScN2a cells were grown and maintained as described[11]. Twenty-four hours after splitting, cells were incubated in a fresh medium containing the appropriate concentration of rPrP and/or quinacrine (Sigma, St. Louis, MO) or the same volume of PBS as a negative control and incubated for 3 days. Quinacrine was dissolved in PBS. Cell lysis and proteinase K (PK) digestion were performed as described[12]. PK-insoluble pellets and PK-undigested samples were subjected to 12% SDS-PAGE and Western blotting using standard procedure. Anti-PrP

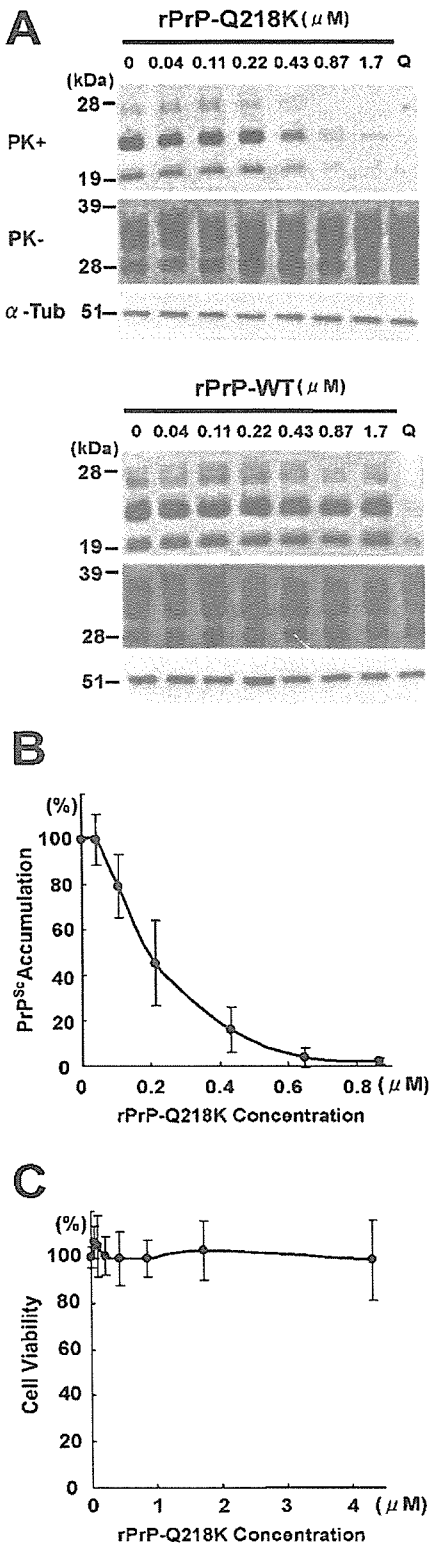

monoclonal antibody (mAb) 6H4 (1:5000; Prionics, Schlieren, Switzerland) or α-tubulin mAb (1 : 10000; DM1A, Sigma) was used as the primary antibody, and horseradish peroxydase-conjugated anti-mouse IgG (1 : 5000; Cappel, West Chester, PA) was used as the secondary antibody. Immunodecorated bands were visualized by the ECL-plus (Amersham Bioscience). For evaluating the accumulation of PrP^{Sc}, the PK-resistant bands were quantified by densitometry (LAS-1000; Fujifilm, Tokyo, Japan). Average values of at least three independent experiments were plotted as percentage of the amount of PrP^{Sc} found in equivalent untreated ScN2a cells on the day of collection.

Cytotoxicity assays

The cytotoxicity of rPrP and quinacrine in ScN2a cells was evaluated by the WST-8 assay (Cell Counting Kit-8, Dojindo Lab, Kumamoto, Japan) measuring the formation of a yellow color formazan dye produced by dehydrogenase activities in viable cells from 2- (2-methoxy-4-nitrophenyl)- 3- (4-nitrophenyl)- 5- (2,4-disulfophenyl)- 2H- tetrazolium, monosodium salt (WST-8). ScN2a cells (4×10^3 cells/well) were cultured at 37°C for 24 h in 96-well plates, incubated in the medium containing the appropriate concentration of drugs for 48 h and were subjected to WST-8 assay according to the manufacturer's protocol.

FIGURE 1: Dose-dependent inhibition of PrP^{Sc} formation in ScN2a cells with rPrP-Q218K. (A) PrP^{Sc} signals in ScN2a culture cells are compared by immunoblotting in the presence of rPrP-Q218K or rPrP-WT at 0 – 1.7 μM (0 - 40 μg/ml). (0) represents untreated cells, and (Q) represents positive controls treated with 1.5 μM of quinacrine. PrP^{Sc} is detected with anti-PrP mAb (6H4) after proteinase K (PK) digestion (20 μg/ml, 1 h, 37°C, 1st row), and total PrP (PrP^{C} and PrP^{Sc}) is detected without PK digestion (2nd row). After incubation with rPrP-Q218K, PrP^{Sc} in ScN2a cells is reduced in a dose-dependent manner, whereas the administration of rPrP-WT by up to 1.7 μM (40 μg/ml) does not change PrP^{Sc} formation. Total PrP remains unchanged in both treatments. The same undigested cell lysates are stained with αtubulin mAb (DM1A, Sigma, St. Louis, MO). (B) Densitometric measurements of PrP^{Sc} signals in panel A. All data represent the mean values (± SD) from at least three independent experiments. (C) Cell viability is determined by the WST-8 assay, in which the absorbance values indicate the yield of colored formazan in proportion to total number of viable cells. Each point represents the mean absorbance value (± SD) calculated from four sets of experimental data. Up to 4.3 μM (100 μg/ml) of rPrP-Q218K doesn't reduce the viability of ScN2a cells.

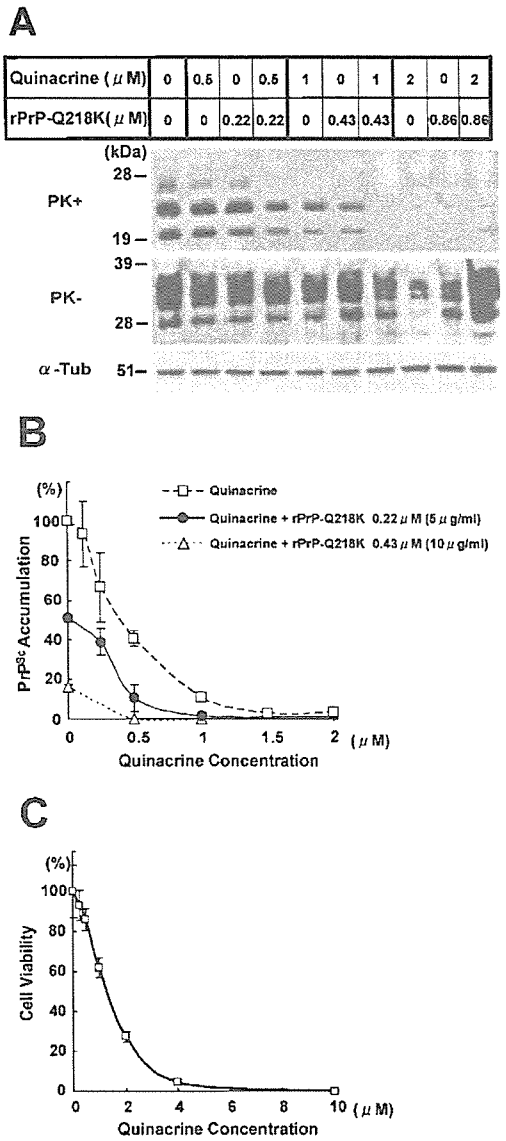

FIGURE 2: Additive inhibition of PrP^{Sc} formation by the combination of rPrP-Q218K and quinacrine. (A) PrP^{Sc} signals in ScN2a cells are compared by immunoblotting in the presence of quinacrine and/or rPrP-Q218K (see legend to Figure. 1A). PrP^{Sc} level in ScN2a cells is additively reduced. (B) Densitometric measurements of PrP^{Sc} signals in panel A (see legend to Figure. 1B). Open squares, quinacrine; filled circles, quinacrine with 0.22 μM (5 μg/ml) of rPrP-Q218K; open triangles, quinacrine with 0.43 μM (10 μg/ml) of rPrP-Q218K. The inhibition on PrP^{Sc} formation with quinacrine with rPrP-Q218K is more effective than that of quinacrine alone. (C) Cell viability is determined by the WST-8 assay (see legend to Figure. 1C). The treatment of quinacrine damages the cell viability in a dose-dependent manner.

Immunofluorescent microscopy

For indirect immunofluorescence analysis, mouse neuroblastoma (N2a) cells grown on glass cover slips in the presence of 0.43 μM (10 μg/ml) of rPrP with 3F4 epitope (MHM2 rPrP) for 3 h were rinsed with PBS without Ca^{2+} and Mg^{2+} (PBS(−)) and then fixed with 2% formalin in 70% PBS(−) for 15 min at room temperature. After four washes, the fixed cells were incubated 10% FBS in PBS(−) for 30 min at room temperature. They were then incubated for 1 h at room temperature with anti-SHaPrP 3F4 mAb (1:200; Sigma) and anti-asialo-GM1 antibody (1:200, CALBIOCHEM, La Jolla, CA) as a marker of rafts. After four washes with PBS (−), the cells were incubated with Alexa 488 Fluor-conjugated goat anti-mouse IgG (1 : 500, Molecular Probes, Eugene, OR) and Alexa 594 Fluor-conjugated goat anti-rabbit IgG (1 : 100, Molecular Probes) for 1 h at room temperature. The cells were washed 4 times with PBS(−) and mounted with SLOW FADE (Molecular Probes) and observed using Delta Vision Microscope Systems (Applied Precision, LLC).

Surface plasmon resonance (SPR) measurement

A BIAcore 3000 system (BIAcore AB, Uppsala, Sweden) was used to analyze molecular interactions by means of SPR. rPrP-WT at 500 μg/ml was diluted 1:10 with 10 mM sodium acetate buffer at pH 6.0 and immobilized to a sensor chip CM5 (carboxymethylated dextran surface) using amine coupling according to the manufacture's instructions. Samples for analyte proteins were diluted ($3.2 \times 10^{2 \sim 0}$ μg/ml) in the running buffer (10 mM HEPES-KOH, pH 7.4, 150 mM NaCl, 3 mM EDTA, 0.005% Surfactant P20), and injected over the surface at 4°C with a flow rate of 20 μl/min. Each sensorgram was subtracted for the response observed in the control flow cell containing a blank surface and results were analyzed by using BIA evaluation SPR kinetic software (BIAcore).

Results

Purified rPrP-Q218K or rPrP-WT was added into the culture media of ScN2a cells at the designated concentrations and incubated for 3 days (see Materials and methods). Ultracentrifugation using a sucrose density gradient revealed that these rPrPs were monomeric (data not shown). While PrP^{Sc} formation was not altered by up to 1.7 μM (40 μg/ml) of rPrP-WT (Figure 1A), it was dramatically reduced in rPrP-Q218K-treated ScN2a cells; 50% effective concentration (EC_{50}) was 0.19 μM (4.5 μg/ml) and EC_{99} was 0.86 μM (20 μg/ml) (Figure 1B) in a concentration-dependent manner (Figures 1A, 1B). Of

note, the viability of ScN2a cells measured with WST-8 assay was not reduced up to 5-fold higher concentrations than EC_{99} of rPrP-Q218K (Figure 1C). On the contrary, quinacrine reduced viability of ScN2a cells by 50% at the concentration of EC_{99} (1.5 μM) (Figure 2C). As previously demonstrated[13,14], quinacrine inhibited PrP^{Sc} formation in ScN2a cells (EC_{50} = 0.45 μM, EC_{99} = 1.5 μM) but less efficiently.

When both rPrP-Q218K and quinacrine were applied onto ScN2a cells simultaneously, an additive inhibitory effect was observed. After the combined administration of 0.5 μM of quinacrine and 0.22 μM (5 μg/ml) of rPrP-Q218K, PrP^{Sc} formation in ScN2a cells was reduced by another 30% compared with quinacrine alone (Figure 2A, 2B). When combined with 0.43 μM (10 μg/ml) of rPrP-Q218K, EC_{99} of quinacrine was also decreased from 1.5 μM to 0.5 μM, in which the cell viability was recovered from 50% to over 90% as inversely proportional to the concentration of quinacrine (Figure 2C).

In order to gain further mechanistic insight into the inhibition of PrP^{Sc} formation by rPrP-Q218K, morphological and biochemical analyses were performed. Indirect immunofluorescent microscopy detected these rPrPs on the cell surface with no difference in distribution profiles (Figure 3). These results show that some factor/s other than the GPI-anchor rendered the rPrPs detected on the cell surface.

SPR measurement revealed that both analytes of rPrP-Q218K and rPrP-WT did not bind to rPrP-WT immobilized onto the chip surface as a ligand, whereas anti-prion mAb 6H4 bound the ligand of rPrP at the equilibrium dissociation constant (K_D) of 2.2 x 10^{-9}. In order to correct the instrumental noise and non-specific binding, the sensorgram of the flow cell containing rPrP-WT-immobilized sensor chip was subtracted from that of a blank cell. However, SPR could not detect any interaction between amine-coupled rPrP-WT on the surface of the chip and soluble rPrP-Q218K/rPrP-WT in the flow, indicating their KD values below the detection limit of SPR measurement.

Discussion

While mouse Q218K in a GPI-anchored form has already been known as a dominant negative in ScN2a culture cells[6,7] and transgenic mice[8], we have demonstrated that the administration of non-GPI-anchored rPrP-Q218K sufficiently inhibits PrP^{Sc} formation in ScN2a cells for the first time.

Meier *et al.* recently reported that soluble wild-type PrP derivatives might represent a new class of prion replication antagonists with transgenic and gene knockout approaches[15]. In PrP transgenic mice with a wild-type background, the expression of PrP^{C} rendered soluble and dimeric by fusion to immunoglobulin Fcγ (PrP-Fc2) delays PrP^{Sc} accumulation, agent replication, and onset of disease following inoculation with infective prions. While it is preliminary to consider such gene therapeutics, *e.g.* an *ex vivo* gene transfer approach[16,17], the direct administration of soluble rPrPs such as our rPrP-Q218K would be an alternative approach for prion therapeutics. In addition, homogeneous and high-quality soluble rPrP-Q218K could be easily prepared from large-scale fermentation of *E. coli* in sufficient quantities.

Artificial administration of anti-PrP antibodies have been shown to exert a protective effect against infection with PrP^{Sc} [18,19], which is in good agreement with our own data *in vitro*; EC_{50} of anti-PrP antibody Fab D18 (kindly provided by Dr. Stanley B. Prusiner) = 6 nM, and EC_{99} = 30 nM (data not shown). However, a recent clinical trial of Aβ vaccination targeting Alzheimer's disease has been halted due to the serious neurological complications of autoimmune reactions developing in

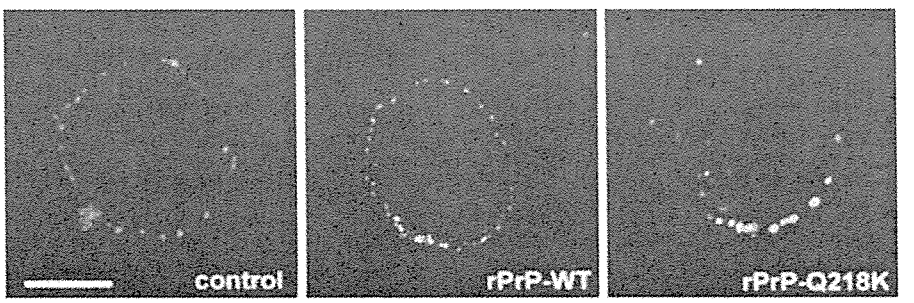

FIGURE 3: Both rPrP-WT and rPrP-218K bind to N2a cells. N2a cells are incubated for 3 h with PBS(−), 10 μg/ml rPrP-WT or rPrP-Q218K, washed with PBS(−), fixed with 2% formalin, and subjected to indirect immunofluorescent microscopy. rPrPs, asialo-GM1 are displayed in green and red, respectively. PrP^{C} and asialo-GM1 are localized on the plasma membrane. Both rPrPs are detected on a part of lipid rafts. Bar: 15 μm.

some patients[20,21]. In contrast, the generation of anti-PrP antibodies *in vivo* has proven quite difficult in wild-type animals, PrP being a notoriously poor immunogen[22]. From the aspect of avoiding such unwanted autoimmune reactions, rPrPs might also be considered as a better candidate for prion therapeutics.

Quinacrine, an anti-malarial drug, was reported to inhibit PrP^{Sc} formation in ScN2a cells[13,14], and has already been prescribed for CJD patients in a tentative way[23]. Unfortunately, quinacrine tends to provoke a drug-induced liver dysfunction[24], which frequently forces cessation of the drug administration. In order to minimize the side effects of quinacrine, we expected that combination treatment of multiple anti–prion drugs might be an alternative option. In fact, when combined with rPrP-Q218K, the EC_{99} of quinacrine was successfully reduced and no significant cytotoxicity was observed at the same range of concentration in ScN2a cells. Such a combination could alleviate the side effects of quinacrine by reducing its effective concentration without changing or even accelerating the inhibition efficacy.

Enari *et al.*[25] proposed that sequestration of PrP^{C} by anti-PrP antibody or removal by phosphatidyl-inositol specific phospholipase C (PIPLC) leads to depletion of PrP^{Sc} due to much more rapid turnover of PrP^{Sc} than previously supposed. Since decrease in PrP^{C} by administration of rPrP-Q218K to ScN2a cells was not detected (Figure 1A), the inhibition of PrP^{Sc} accumulation seems to be caused by secession of PrP^{Sc} synthesis, stimulation of PrP^{Sc} degradation or a combination of both.

It was shown that both rPrP-Q218K and rPrP-WT in non-GPI-anchored form were equally detectable on the cell surface, where the conversion of PrP^{C} into PrP^{Sc} takes place[26,27]. Of note, such equal binding seems to be independent of the inhibition of PrP^{Sc} formation, since only rPrP-Q218K but not rPrP-WT exclusively inhibited the PrP^{Sc} formation in ScN2a cells. Nonetheless, one might assume that rPrP-Q218K aberrantly binds to endogenous PrP^{C} in terms of the binding partner, which is undetectable by the conventional immunofluorescent microscopy, and concurrently inhibits PrP^{Sc} formation. Real-time kinetics analysis by SPR, however, failed to detect any significant difference in the binding kinetics of rPrP-WT as a ligand with rPrP-WT or rPrP-Q218K as analytes. Measurements of on-rates (ka) and off-rates (kd) of protein-protein interactions made by SPR is extremely sensitive, and these values are directly related to KD[28]. Taken into account the fact that SPR successfully detects binding interactions in the order of 10^{-3}~$^{-4}$ of KD[28], it seems less likely that such discrepancy between rPrP-Q218K and rPrP-WT on the PrP^{Sc} inhibition could be explained by the different binding kinetics of these rPrPs against PrP, although rPrP may not perfectly substitute for PrP^{C}. Instead, it seems likely that these rPrPs more readily interact with a binding factor/s other than PrP where rPrP-Q218K and rPrP-WT are equally detected but inhibit PrP^{Sc} formation differently. Legname *et al.*[29] recently reported that the dominant-negative MoPrP (MoPrP-Q218K)-Fc, in which the C-terminus of MoPrP was fused to the Fc portion of an IgG, not only binds to granule cells but also binds to neurons of the molecular layer where PrP^{C} is expressed, and assuming that the cells of the molecular layer express an auxiliary protein/s, provisionally designated protein X[6,30], which is involved in prion replication. Identification of such factor/s remains to be further examined.

Acknowledgments

We thank Drs. Naoko Iwanami, Yuko Nakamura, and Ken'ichi Hagiwara for useful discussions and Dr. Tamaki Muramoto for providing ScN2a culture cells. This work was supported in part by grants from the Ministry of Health, Labor and Welfare of Japan (14161301), and Core Research for Evolutional Science and Technology (CREST), Japan Science and Technology Corporation.

References

1 Prusiner SB (2001). Shattuck lecture—neurodegenerative diseases and prions. *N Engl J Med* **344**, 1516-1526
2 Collinge J (1999). Variant Creutzfeldt-Jakob disease. *Lancet* **354**, 317-323
3 Prusiner SB (1998). Prions. *Proc Natl Acad Sci USA* **95**, 13363-13383
4 Kitamoto T and Tateishi J (1994). Human prion diseases with variant prion protein. *Philos Trans R Soc Lond B* **343**, 391-398
5 Shibuya S, Higuchi J, Shin RW, Tateishi J and Kitamoto T (1998). Codon 219 Lys allele of PRNP is not found in sporadic Creutzfeldt-Jakob disease. *Ann Neurol* **43**, 826-828
6 Kaneko K, Zulianello L, Scott M, Cooper CM, Wallace AC, James TL, Cohen FE and Prusiner SB (1997). Evidence for protein X binding to a discontinuous epitope on the cellular prion protein during scrapie prion propagation. *Proc Natl Acad Sci USA* **94**, 10069-10074
7 Zulianello L, Kaneko K, Scott M, Erpel S, Han D, Cohen FE and Prusiner SB (2000). Dominant-negative inhibition of prion formation diminished by deletion mutagenesis of the prion protein. *J Virol* **74**, 4351-4360
8 Perrier V, Kaneko K, Safar J, Vergara J, Tremblay P, DeArmond SJ, Cohen FE, Prusiner SB and Wallace AC (2002). Dominant-negative inhibition of prion replication in transgenic mice. *Proc Natl Acad Sci USA* **99**,13079-13084

9 Scott MR, Köler R, Foster D and Prusiner SB (1992). Chimeric prion protein expression in cultured cells and transgenic mice. *Protein Sci* **1**, 986-997

10 Rogers M, Serban D, Gyuris T, Scott M, Torchia T and Prusiner SB (1991). Epitope mapping of the Syrian hamster prion protein utilizing chimeric and mutant genes in a vaccinia virus expression system. *J Immunol* **147**, 3568-3574

11 Butler DA, Scott MA, Bockman JM, Borchelt DR, Taraboulos A, Hsiao KK, Kingsbury DT and Prusiner SB (1988). Scrapie-infected murine neuroblastoma cells produce protease-resistant prion proteins. *J Virol* **62**, 1558-1564

12 Korth C, Kaneko K and Prusiner SB (2000). Expression of unglycosylated mutated prion protein facilitates PrP(Sc) formation in neuroblastoma cells infected with different prion strains. *J Gen Virol* **81**, 2555-2563

13 Doh-Ura K, Iwaki T and Caughey B (2000). Lysosomotropic agents and cysteine protease inhibitors inhibit scrapie-associated prion protein accumulation. *J Virol* **74**, 4894-4897

14 Korth C, May BCH, Cohen FE and Prusiner SB (2001). Acridine and phenothiazine derivatives as pharmacotherapeutics for prion disease. *Proc Natl Acad Sci USA* **98**, 9836-9841

15 Meier P, Genoud N, Prinz M, Maissen M, Rulicke T, Zurbriggen A, Raeber AJ and Aguzzi A (2003). Soluble dimeric prion protein binds PrP(Sc) *in vivo* and antagonizes prion disease. *Cell* **113**, 49-60

16 Corbel SY and Rossi FM (2002). Latest developments and in vivo use of the Tet system: ex vivo and in vivo delivery of tetracycline-regulated genes. *Curr Opin Biotechnol* **13**, 448-452

17 Kapturczak MH, Flotte T and Atkinson MA (2001). Adeno-associated virus (AAV) as a vehicle for therapeutic gene delivery: improvements in vector design and viral production enhance potential to prolong graft survival in pancreatic islet cell transplantation for the reversal of type 1 diabetes. *Curr Mol Med* **1**, 245-258

18 Peretz D, Williamson RA, Kaneko K, Vergara J, Leclerc E, Schmitt-Ulms G, Mehlhorn IR, Legname G, Wormald MR, Rudd PM, Dwek RA, Burton DR and Prusiner SB (2001). Antibodies inhibit prion propagation and clear cell cultures of prion infectivity. *Nature* **412**, 739-743

19 White AR, Enever P, Tayebi M, Mushens R, Linehan J, Brandner S, Anstee D, Collinge J and Hawke S (2003). Monoclonal antibodies inhibit prion replication and delay the development of prion disease. *Nature* **422**, 80-83

20 Dodart JC, Bales KR and Paul SR (2003). Immunotherapy for Alzheimer's disease: will vaccination work? *Trends Mol Med* **9**, 85-87

21 McGeer PL and McGeer E (2003). Is there a future for vaccination as a treatment for Alzheimer's disease? *Neurobiol Aging* **24**, 391-395

22 Koller MF, Grau T and Christen P (2002). Induction of antibodies against murine full-length prion protein in wild-type mice. *J Neuroimmunol* **132**, 113-116

23 Follette P (2003). New perspectives for prion therapeutics meeting. Prion disease treatment's early promise unravels. *Science* **299**, 191-192

24 Scoazec JY, Krolak-Salmon P, Casez O, Besson G, Thobois S, Kopp N, Perret-Liaudet A and Streichenberger N (2003). Quinacrine-induced cytolytic hepatitis in sporadic Creutz-feldt-Jakob disease. *Ann Neurol* **53**, 546-547

25 Enari M, Flechsig E and Weissmann C (2001). Scrapie prion protein accumulation by scrapie-infected neuroblastoma cells abrogated by exposure to a prion protein antibody. . *Proc Natl Acad Sci USA* **98**, 9295-9299

26 Taraboulos A, Scott M, Semenov A, Avrahami D, Laszlo L and Prusiner SB (1995). Cholesterol depletion and modification of COOH-terminal targeting sequence of the prion protein inhibit formation of the scrapie isoform. *J Cell Biol* **129**, 121-132

27 Kaneko K, Vey M, Scott M, Pilkuhn S, Cohen FE and Prusiner SB (1997). COOH-terminal sequence of the cellular prion protein directs subcellular trafficking and controls conversion into the scrapie isoform. *Proc Natl Acad Sci USA* **94**, 2333-2338

28 Myszka DG (1997). Kinetic analysis of macromolecular interactions using surface plasmon resonance biosensors. *Curr Opin Biotechnol* **8**, 50-57

29 Legname G., Nelken P, Guan Z, Kanyo ZF, DeArmond SJ and Prusiner SB (2002). Prion and doppel proteins bind to granule cells of the cerebellum. *Proc Natl Acad Sci USA* **99**, 16285-16290

30 Telling GC, Scott M, Mastrianni J, Gabizon R, Torchia M, Cohen FE, DeArmond SJ and Prusiner SB (1995). Prion propagation in mice expressing human and chimeric PrP transgenes implicates the interaction of cellular PrP with another protein. *Cell* **83**, 79-90

Articles

Slow Conformational Dynamics in the Hamster Prion Protein†

Kazuo Kuwata,*,# Yuji O. Kamatari,⊥ Kazuyuki Akasaka,‡ and Thomas L. James*,§

Department of Biochemistry and Biophysics, School of Medicine, Gifu University, Gifu 500-8705 Japan, Cellular Signaling Laboratory, RIKEN Harima Institute, Hyogo, 679-5148 Japan, Department of Biotechnological Sciences, School of Biology-Oriented Science and Technology, Kinki University, Wakayama, 649-6493 Japan, and Department of Pharmaceutical Chemistry, 600 16th Street, Genentech Hall, University of California, San Francisco, California, 94143-2280 USA

Received November 25, 2003; Revised Manuscript Received February 9, 2004

ABSTRACT: Although the mechanism of the conformational conversion from the cellular (PrP^C) to the scrapie (PrP^{Sc}) form of animal prion proteins has yet to be elucidated, evidence is accumulating that may provide insight into the conversion process at atomic resolution. Here we show critical aspects of the slow fluctuation dynamics of the recombinant hamster prion protein, rPrP(90−231), based on NMR relaxation analysis using Carr-Purcell-Meiboom-Gill (CPMG) experiments, and compare them in detail with results from high-pressure NMR. Residues exhibiting slow fluctuations on the time scale of microseconds to milliseconds are mainly localized on helices B and C (172−193 and 200−227), which include locally disordered regions in an intermediate conformer, PrP*, identified previously by high-pressure NMR [Kuwata, K., et al., (2002) *Biochemistry* 41, 12277−12283]. Moreover, chemical shift differences between two putative exchanging conformers obtained by the CPMG relaxation analysis and the linear component of the pressure-induced chemical shift changes are reasonably correlated at individual residue sites. These observations suggest that both the CMPG relaxation and the pressure shifts reflect slow conformational fluctuations and that these slow motions in PrP^C are related to the trajectories leading to the transition to PrP*.

Prions cause neurodegenerative diseases, such as scrapie in sheep, bovine spongiformencephalopathy (BSE) in cattle, Creutzfeldt-Jakob disease (CJD), Gerstmann-Sträussler-Scheinker syndrome (GSS), fatal familial insomnia (FFI), kuru, and a new variant of CJD in humans (*1*−*3*). These diseases are associated with conversion of the normal cellular form of the prion protein (PrP^C) to a pathogenic scrapie form (PrP^{Sc}), which is apparently the infectious agent in transmitted forms of the disease (*3*, *4*). The sequences of PrP^{Sc} and the noninfectious precursor PrP^C are identical (*5*). Although both isoforms are chemically identical, they possess very different physicochemical properties. PrP^C is substantially helical, but PrP^{Sc} has ~40% β-sheet (*6*).

The three-dimensional structure of PrP^C was first elucidated for the mouse, Mo PrP (121−231) (*7*), and the hamster species, SHa PrP (90−231) (*8*), by NMR. Subsequently, structures for bovine (*9*) and human (*10*) species were elucidated. While there are some species-specific differences, the structures are similar in that residues 128−231 constitute a globular fold with three α-helices, a small, imperfectly formed and conformationally flexible β-sheet composed of antiparallel strands S1 and S2, an N-terminal segment up to residue 113 completely disordered and, at least in the hamster species, a hydrophobic cluster (residues 113−128) with multiple interconverting conformers (*11*).

NMR studies of dynamics in the PrP^C structure were reported (*11*, *12*) using heteronuclear NOE, T_1, T_2, and off-resonance $T_{1\rho}$ relaxation time measurements (*12*). The results are consistent with the static picture of PrP^C, i.e., the central portions of helices B and C form a relatively rigid core, but the remainder of the globular domain and helix A are more flexible on a picosecond-to-nanosecond time scale. Slow conformational fluctuations on the microsecond-to-millisecond time scale were observed only for the small β-sheet and the hydrophobic cluster (*11*, *12*).

However, our recent results for conformational fluctuations by high-pressure NMR were quite different from that static picture, possibly due to the difference in the time scale of the fluctuations (*13*). Consequently, here we examined NMR relaxation results for SHa PrP (90−231) using the Carr-Purcell-Meiboom-Gill (CPMG) method (*14*) as well as standard T_1, T_2, and NOE measurements, together with a

† Supported in part by Grants-in-Aid for Scientific Research from the Ministry of Education, Culture, Sports, Science and Technology of Japan (14380314, 14037224) and by the Gifu Prefecture Brain Research Foundation.

* To whom correspondence should be addressed. E-mail: james@picasso.ucsf.edu; tel.: (415) 476-1916; fax: (415) 502-8298 or e-mail: kuwata@cc.gifu-u.ac.jp; tel: +81-582-67-2227; fax: +81-582-67-2962.

Gifu University.

⊥ RIKEN Harima Institute.

‡ Kinki University.

§ University of California.

10.1021/bi036123o CCC: $27.50
Published on Web 03/26/2004

further detailed analysis of the high-pressure NMR results. All of these data pertaining to prion protein dynamics are examined in the context of biological and clinical observations (*15*).

MATERIALS AND METHODS

Samples. Expression, isotopic labeling, purification, and considerations for proper refolding of recombinant Syrian hamster prion protein rPrP (90−231) have been described previously (*11*, *13*). Purified rPrP (90−231), labeled uniformly with ^{15}N, was lyophilized before refolding. Samples were analyzed by mass spectroscopy, circular dichroism, and Fourier transform infrared spectroscopy to ensure the refolded rPrP (90−231) resembles PrP^C, i.e., is largely α-helical.

NMR Measurements. The online high-pressure NMR system contains the protein solution in a quartz tube cell that endures pressures of ≥2500 bar. The cell was connected to a high-pressure line via frictionless Teflon pistons that separate the protein solution from the pressure mediator (kerosene) in a separator cylinder (BeCu). The cell body (inner diameter 1 mm, outer diameter 3 mm) is positioned in a commercial 5-mm NMR probe (Bruker). Pressure was regulated to a desired value between 1 and 2500 bar with a remote hand-pump and maintained at that value during signal accumulation. For 1D and 2D NMR measurements, samples were dissolved in 95% ^1H_2O/5% ^2H_2O containing 20 mM sodium acetate, pH 5.2, to make a 1 mM protein solution. As chemical shift references, trace amounts of sodium 3-trimethylsilyl-(2,2,3,3-^2H)-tetradeuteriopropionate (TSP-d_4) and dioxane were added to the solution. The dioxane resonance remains unchanged with pressure (3.750 ppm from TSP at 1 bar). Relaxation time measurements were performed in standard Shigemi tubes with 11.7 T (Varian Inova 500) and 18.8 T NMR spectrometers (Bruker Avance 800).

Reduced Spectral Density Mapping. ^{15}N longitudinal (T_1) and transverse (T_2) relaxation times and {^1H}-^{15}N heteronuclear NOEs were measured using two different magnetic fields, 11.7 T (500 MHz proton frequency) and 18.8 T (800 MHz). Several peaks are overlapped and are not presented here. For residues 100−231, the R_1 (=$1/T_1$) rates are relatively invariant around 1.5 s^{-1} at 11.7 T. At 18.8 T, for residues 128−231, they are all approximately 1.0 s^{-1}. For residues 100−110, R_1 values are about 1.5 s^{-1}, indicating the relative invariance to the magnetic field strength, which is commonly observed for natively unfolded protein (*16*, *17*). The reduced spectral density function, $J(\omega)$, provides insights into the motion of the N−H bond vector at five frequencies: 0, ω_{N1} (0.32 gigaradian (grad)/s), ω_{N2} (0.51 grad/s), $0.87\omega_{H1}$ (2.73 grad/s), and $0.87\omega_{H2}$ (4.37 grad/s), where 1 and 2 denote angular velocities at 11.7 and 18.8 T, respectively. The largest value of $J(0)$ is ~6 ns at 11.7 T and ~5 ns at 18.8 T. The different $J(0)$ values at 11.7 and 18.8 T demonstrate the inherent limitation of deriving absolute $J(0)$ values from first-order reduced spectral density mapping. The $J(0)$ values at 11.8 T are used in Figure 6a (vide infra).

Slow Fluctuation Analysis. Values of the exchange lifetime τ_{ex} were calculated from the dependence of the signal intensities on interpulse spacing in the CPMG experiment (*13*, *14*). The pulse sequence for measuring the ^{15}N R_2 values (*18*−*20*) was used with modifications for averaging in-phase and antiphase coherence (*21*, *22*).

The apparent transverse relaxation rate with two-site chemical exchange can be expressed as (*14*)

$$R_2^* = R_2 + \tau_{ex} f_1 f_2 (\Delta\omega)^2 \left[1 - \frac{2\tau_{ex}}{\tau_{cp}} \tanh\left(\frac{\tau_{cp}}{2\tau_{ex}}\right)\right] \quad (1)$$

where τ_{cp} is the delay between 180° pulses in the CPMG sequence, and $\Delta\omega$ is the difference in chemical shift of the nucleus in the two conformational states. τ_{ex} (= $\tau_{-1}f_1 = \tau_1 f_2$) is the exchange time constant. f_1 and f_2 (= $1 - f_1$) are the fractions of populations of the two conformational states, and τ_1 and τ_{-1} are forward and the reverse exchange time constants, respectively. R_2 is the pure transverse relaxation rate due to the molecular motion on the time scale of picoseconds to nanoseconds without the slow exchange contribution on the microsecond-to-millisecond time scale. Numerical calculation using the exact equation (*23*) shows that eq 1 is accurate within 5% when $\Delta\omega < 4$ ppm and $\tau_{cp}/\tau_{ex} < 10^{-2}$. In our case, $(f_1 f_2)^{1/2}\Delta\omega \sim 0.1$ kHz, and $\tau_{ex} \sim 0.002$ s. However, since the exact equation is still a monotonic function of $\Delta\omega$ and τ_{ex}, we may be able to characterize these parameters qualitatively rather than quantitatively, even when $(f_1 f_2)^{1/2}\Delta\omega > 0.1$ kHz, and $\tau_{ex} > 0.002$ s. This is illustrated by representative examples of nonlinear fits that are shown in Supporting Information.

High-Pressure NMR Analysis. In general, the conformation of a protein molecule in solution may consist of an equilibrium mixture of conformers differing in topology of folding (e.g., between the native conformer N and an intermediate partially folded conformer I), in partial molar volume V, as well as in thermodynamic stability ΔG. In this situation, the equilibrium constant K between N and I may change with pressure according to the relation:

$$K = [I]/[N] = \exp(-\Delta G/RT) \quad (2)$$

where

$$\Delta G = G(I) - G(N) = \Delta G_0 + \Delta V(p - p_0) - (1/2)\Delta\beta V (p - p_0)^2 \quad (3)$$

ΔG and ΔG_0 are the Gibbs free energy changes from N to I at pressure p and p_0 (= 1 bar), respectively, ΔV is the partial molar volume change, $\Delta\beta$ is the change in compressibility coefficient, R is the gas constant, and T is the absolute temperature (*13*).

The pressure dependence of the chemical shifts was analyzed according to

$$\delta_i = a_i + b_i p + c_i p^2 \quad (4)$$

where δ_i is the chemical shift for the ith residue, and a_i, b_i, and c_i are independent linear and nonlinear coefficients of the pressure-induced shift, respectively.

Curve fitting was performed using SigmaPlot2001 (SPSS Science, Chicago, IL) on all observed data.

RESULTS

Spectral Densities. First, we measured the reduced spectral density function (*18*), $J(\omega)$, for almost all residues of PrP^C, which would provide insights into the motion of the N−H bond vector at five frequencies 0, 0.32, 0.51, 2.73, and 4.37

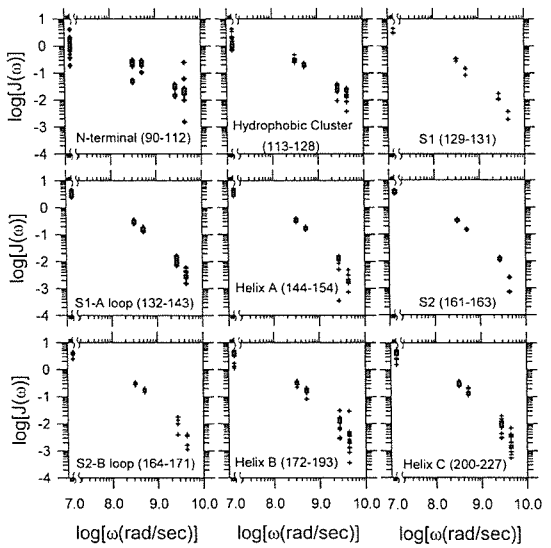

FIGURE 1: The reduced spectral density function, $J(\omega)$, of the N−H bond vector is shown for different regions of PrP^C at five frequencies: 0, ω_{N1} (0.32 grad/s), ω_{N2} (0.51 grad/s), $0.87\omega_{H1}$ (2.73 grad/s), and $0.87\omega_{H2}$ (4.37 grad/s), where subscripts 1 and 2 denote angular velocities at 11.7 and 18.8 T, respectively.

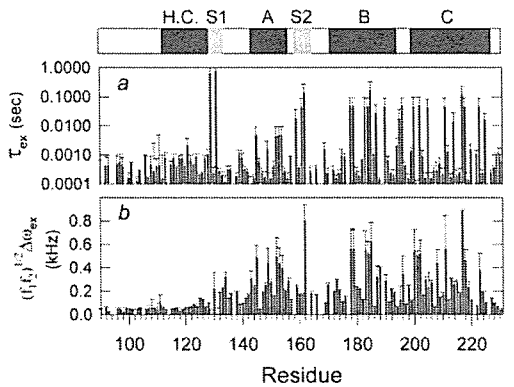

FIGURE 2: (a) Slow exchange lifetimes (τ_{ex}) obtained using the CPMG dispersion method (*14*) plotted as a function of residue number. (b) $\{f_1f_2\}^{1/2}\Delta\omega_{ex}$ plotted as a function of residue number. $\Delta\omega_{ex}$ is the difference in chemical shift of the nucleus in the two conformational states. f_1 and f_2 (= $(1 - f_1)$) are the populations of the two conformational states.

gigaradian (grad)/s using two static magnetic field strengths, 11.7 and 18.8 T. As shown in Figure 1, $J(0)$ values for the N-terminal and hydrophobic cluster are relatively low and rather dispersed, while those for residues in S1 and S2 β-strands and helices B and C are comparatively high. Large $J(0)$ values reflect the global tumbling motion (*12*). We note that J (4.37 grad/s) values are also quite heterogeneous for N-terminal regions and helices B and C, suggesting a large degree of flexibility.

Slow Exchange Dynamics. We obtained evidence of slow conformational exchange from the τ_{cp} dependence of the CPMG dispersion experiments. By assuming two-site exchange, we apply eq 1 (see Materials and Methods) to the CPMG relaxation dispersion data. Figure 2a shows lifetimes corresponding to the slow exchange rates obtained (*14*). Values for the slow exchange time constant, τ_{ex}, and the

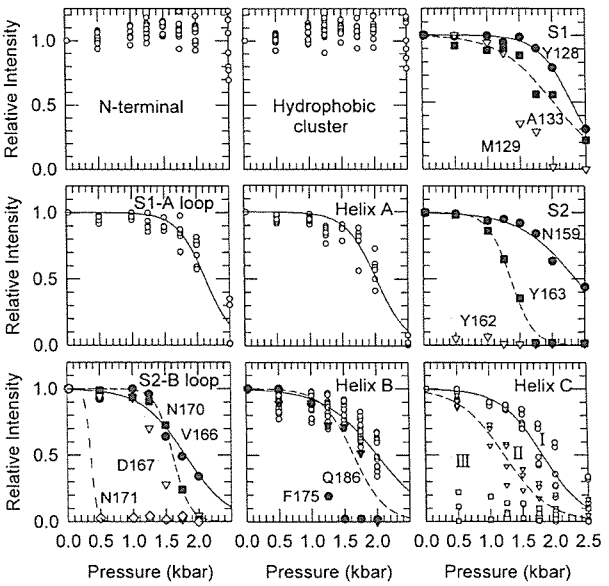

FIGURE 3: Integrated intensities of amide resonances in HSQC spectra as a function of pressure. The transition profiles are divided into nine groups according to secondary structure elements of PrP^C. The multiple values at each pressure correspond to different residues within a structural region. Lines are from curve fitting using eq 2. The transition from the native conformation varies from site to site, showing that the pressure stability of rPrP(90−231) is site-dependent.

difference in chemical shifts ($\Delta\omega$), shown in Figure 2b, were calculated using eq 1. The τ_{ex} values are on the microsecond-to-millisecond time scale, and the relatively large $\Delta\omega$ values are mainly found in the β-strands S1 and S2 and helices B and C. Specifically, residues with τ_{ex} larger than 0.01 s are M129, G131, N159, V161, Y162, D178, C179, T183, I184, L185, H187, T190, G195, E196, E200, D202, I205, E211, C214, Q217, Y218, Q223, and Y225. They are mapped by yellow in Figure 4a.

High-Pressure NMR. Under high pressure, the population of the native state is generally decreased and, if present at all, that of an intermediate state is increased, because the partial molar volume of the native structure is generally larger than that of the intermediate structure, since it is presumably less tightly folded. Pressure-induced conformational transitions are generally less cooperative than those of other perturbations, such as temperature or denaturant concentration, because, in the native conformation, each affected residue is adjacent to a cavity with specific volume. Therefore, pressure-induced disorder of the native conformation often varies from site to site, showing that the thermodynamic stability of rPrP(90−231) is site dependent. We categorized the behaviors of the integrated intensities of amide residues in HSQC spectra as a function of pressure into nine groups according to secondary structure elements of the protein, as shown in Figure 3. Lines are theoretically generated by fitting eq 2, in Materials and Methods, to the experimental data points. Cross-peak intensities from the N-terminus and the hydrophobic cluster were essentially invariant with pressure, while intensities for residues 128−231 dramatically decreased with pressure, almost disappearing by 2500 bar. This indicates that the major conformational changes are occurring. The relative inertness of spectral

features to pressure is a general property of a disordered conformer. There is substantial heterogeneity in pressure stability among the secondary structure elements. The S1-A loop and helix A were most stable with pressure change, and their transitions occurred uniformly over their constituent residues. Pressure-induced transitions of helix B residues also occurred rather uniformly, with the exception of F175 and Q186. The pressure stability is determined mainly by two factors, the stability at 1 bar (ΔG_0) and ΔV, neglecting the $\Delta\beta$ contribution (eq 3). By extrapolating eq 3 to 1 bar and neglecting data for F175 and Q186, we obtain average thermodynamic stabilities ΔG_0 of helix A and helix B at 1 bar to be 5.2 and 3.0 kcal/mol, respectively. The results clearly indicate that helix B has much less stability than helix A. Other secondary structure elements were even less stable against pressure, and their transitions were more heterogeneous. Transitions of residues in β-strands S1 and S2, the S2-B loop and helix C occurred quite heterogeneously at pressures between 500 and 2500 bar. Transitions were most varied for helix C. They are roughly categorized into three groups (see Figure 3); group I (○: composed of most residues), group II (▽; V210, M213, Q217, K220), and group III (□; K204, I205, Q219).

Thermodynamic analysis, extrapolated to 1 bar via eq 2, gave ΔG_0 values of 3.4 kcal/mol for group I and 2.1 kcal/mol for group II. The group II residues are located essentially at the interface with β-strands S1 and S2, suggesting that the apparent low stability arises from increased conformational disorder of these residues relative to strands S1 and S2. K204, I205, Q219 in group III of helix C, Y162 of S2, N171 of the S2-B loop and F175 of helix B were exceptionally unstable and underwent transitions below 1000 bar. Residues M129, Y163, D167, N170, F175, V210, M213, Q217, and K220 exhibited moderate instability and undergo transitions around 1500 bar. They are mapped in magenta and yellow, respectively, on the NMR structure (*11*) in Figure 4b. Although residues with pressure-induced instability are distributed mainly around the interface between S2 and helix C as shown in Figure 4b, those with any significant slow fluctuations with τ_{ex} more than 0.01 s are distributed more widely and cover S1, S2, helices B and C, as shown in Figure 4a.

Correlation between Fluctuation-Induced and Pressure-Induced Chemical Shift Changes. We have compared the fluctuation- and pressure-induced chemical shift changes, since the measurements are not a priori related. Figure 5a is the plot of the chemical shift changes of amide ^{15}N nuclei induced by fluctuation, $\{f_1 f_2\}^{1/2}\Delta\omega_{ex}$, with τ_{ex} larger than 1 ms, against the linear components of the pressure dependence of the ^{15}N chemical shifts (*13*). Although the amplitudes of the former are about 10 times larger than the latter, they are reasonably well correlated. On the other hand, there is no evident correlation between the chemical shift changes of amide ^{15}N nuclei induced by slow exchange fluctuations, $\{f_1 f_2\}^{1/2}\Delta\omega_{ex}$ with τ_{ex} larger than 1 ms, and any (total or nonlinear) component of the pressure dependence of the ^{15}N chemical shifts (data not shown). Correlations between the chemical shift changes of amide ^{15}N nuclei induced by fluctuation, $\{f_1 f_2\}^{1/2}\Delta\omega_{ex}$ with τ_{ex} on the time scale of microsecond and any pressure dependence of the ^{15}N chemical shifts are not evident.

DISCUSSION

Dynamic Features of the Natively Unfolded N-Terminal Region. Since regions in the hydrophobic cluster (113−128) are only transiently folded (*11*), no significant slow dynamics nor any significant conformational transition was observed (Figures 1−3). However, the hydrophobic cluster is apparently necessary for PrP to convert into PrP^{Sc}. For example, transgenic mice with removal of N-terminal residues beyond residue 93 did not support PrP^{Sc} formation. Interestingly, Tg mice expressing PrP(121−231) develop a cerebellar disorder in the neonatal period implying that much, if not all, of the N-terminal moiety of PrP is necessary for normal function (*24*). Deletion of the C-terminal helices also causes a heritable disorder with severe nerve cell loss (*25*). Therefore, we may assume that the hydrophobic cluster functionally lies within the "death domain", which spontaneously forms the killer conformation via intermolecular interactions such as other conformational diseases (*26*), on the condition that this region is accessible to other pertinent molecules.

Hydrogen bonds apparently exist between M129 and Y163 in the small, unstable β-sheet (*11*), so it is not surprising to see in Figure 3 that M129 and Y163 together exhibit a pressure-induced change. The polymorphism of residue 129, being a valine in many humans, results in different disease phenotypes expressed by the D178N mutation shown in Figure 6f, which can be understood in terms of the structure (*11*). Different clinical manifestations and different prion diseases may result from different conformations of PrP^{Sc} being present. The pressure study further indicates that the region of the S1 strand with methionine at residue 129 is inherently unstable. Residue 129 is near D178, with some evidence that the D178 carboxylate is hydrogen bonded to the Y128 ring hydroxyl (*11*), so conformational fluctuations in helix B can propagate into the S1 strand and proximal hydrophobic cluster. Some amides in the ill-formed β-sheet undergo very slow fluctuations (Figures 2 and 6a,b) and are also affected more readily by pressure (Figures 3 and 6c). That is not surprising, as multiple NMR signals were observed for some β-strand residues (*11*). Both observations emphasize that the β-sheet in PrP^{C} is not very stable. Conceivably, the pressure instability of F175 in helix B is also related to comparatively low stability of S2 and S2-B loop.

Slow Dynamics and Stability of the C-Terminal Helical Region. PrP* was first observed as a metastable intermediate during the unfolding process of SHa rPrP(90−231) with guanidinium chloride (*27*). Other observations have supported the existence of intermediate forms of prions (*28*, *29*). Recently, we characterized some structural features of PrP* (*13*). A small amount of PrP* coexists with native PrP^{C} under nearly physiological conditions (pH 5.2, 30 °C, 1 bar) with the pressure-dependence studies, suggesting that PrP* has disordered B and C helices, while helix A is largely intact (*13*). From the pressure dependence of the signal intensities of individual residues for PrP^{C}, the stability difference of $\Delta G_0 = 2.1$ kcal/mol was obtained for group II residues. This indicates that as much as 1−3% of PrP exists as PrP* at ambient temperature and pressure. Assuming that the signals observed are all from PrP^{C}, the present relaxation analysis indicates that PrP^{C} undergoes millisecond fluctuations particularly in the vicinity of helices B and C.

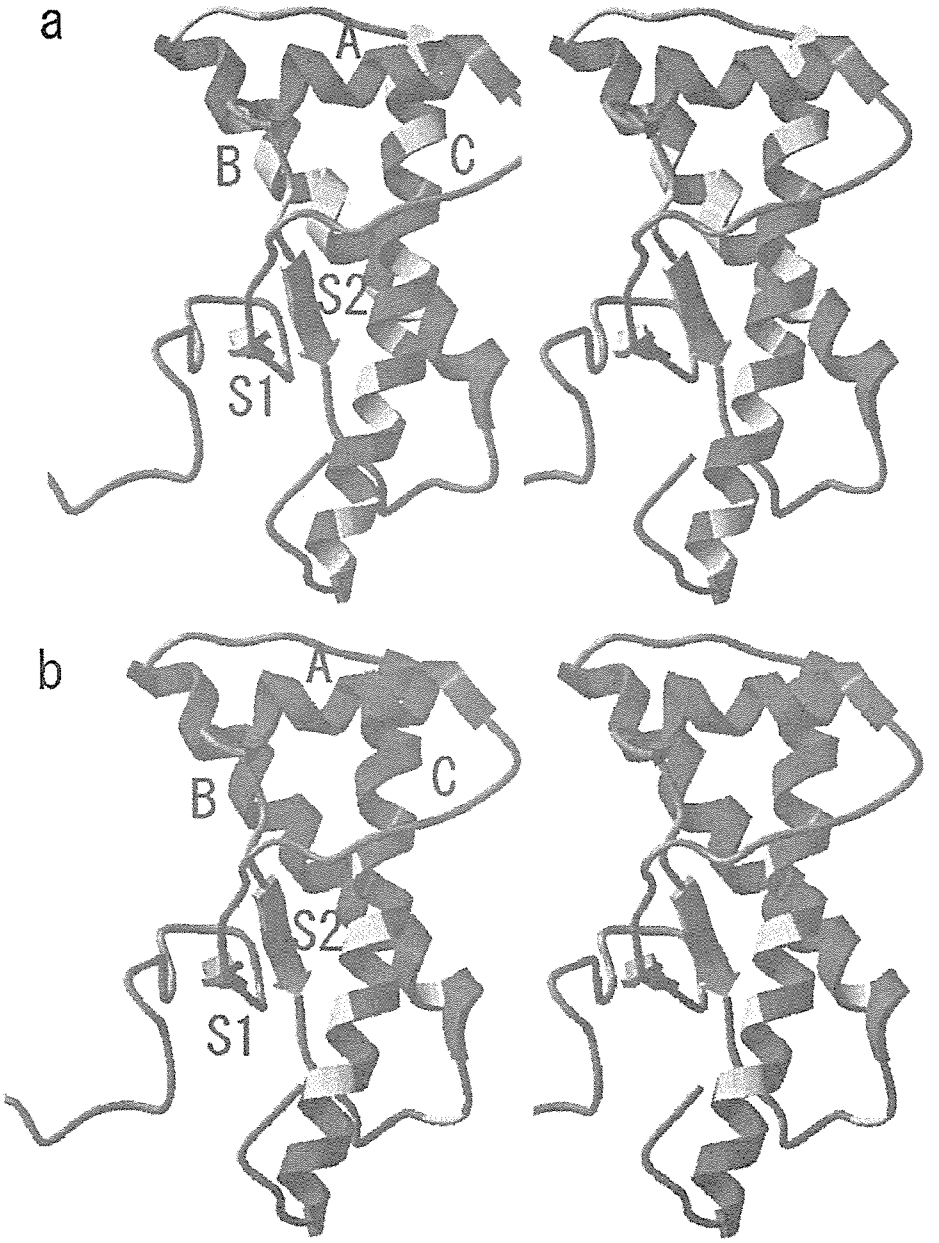

FIGURE 4: In the context of the PrP(90−231) structure, comparison of CPMG T_2 conformational dynamics and high-pressure-induced conformational changes. (a) Residues with τ_{ex} larger than 0.01 s are M129, G131, N159, V161, Y162, D178, C179, T183, I184, L185, H187, T190, G195, E196, E200, D202, I205, E211, C214, Q217, Y218, Q223, Y225, and are mapped in yellow on the NMR structure (*11*). Red represents the helical region, and blue represents other regions. (b) Exceptionally unstable residues that undergo transitions below 1000 bar (K204, I205, Q219 in group III of helix C, Y162 of S2, N171 of the S2-B loop and F175 of helix B), and moderately unstable residues that undergo transitions around 1500 bar (M129, Y163, D167, N170, F175, V210, M213, Q217, and K220) are mapped in magenta and yellow, respectively, on the NMR structure (*11*).

The unstable residues of helices B and C are near a cluster of cavities (*13*), suggesting that the slow dynamics and selective disorder of helices B and C may be related to instability of these cavities. In particular, the HSQC cross-peak intensity reduction observed at relatively low pressures (<500 bar) for group III residue Q219 on helix C is remarkable. As noted previously (*11*), the hamster species, SHa PrP(90−231), and the mouse species, Mo PrP(121−231), differ in that the latter exhibits a break in the helix at Q219. Also, the S2-B loop in SHa PrP (90−231) is well-defined by NMR data but is disordered in Mo PrP (121−231). It should be also noted that Q219 corresponds to the region exhibiting the dominant negative inhibition of prion replication (*26*) (Figure 6d) and also belongs to the protein X binding epitope (*30*) (Figure 6e). Four residues, Q168 in the S2-B loop, Q172 at the beginning of helix B, and T215 and Q219 on helix C, form an epitope that interacts with the putative protein X (*30*), which may well be something other than a protein. Q168, as part of the helical turn, is not in close proximity to the other three residues (Figure 6e).

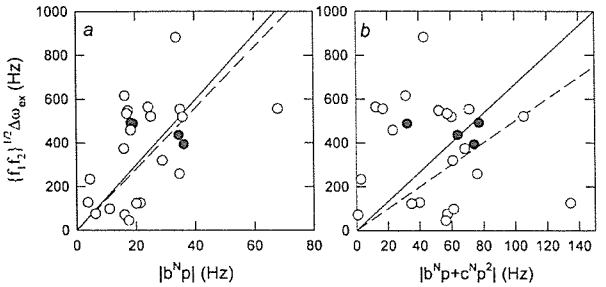

FIGURE 5: Plots of the chemical shift changes of amide ^{15}N nuclei induced by slow fluctuations versus pressure dependencies of the amide ^{15}N chemical shift (*13*). Symbols (○) and (●) indicate residues in helices and in β-sheets, respectively, and lines represent the result of regression analyses. (a) Plot of $\{f_1f_2\}^{1/2}\Delta\omega_{ex}$ for residues with τ_{ex} larger than 1 ms against the linear component of the pressure-dependent chemical shift change of amide ^{15}N resonances. (b) Plot of $\{f_1f_2\}^{1/2}\Delta\omega_{ex}$ for residues with τ_{ex} larger than 1 ms against the total pressure-dependent chemical shift change of amide ^{15}N resonances.

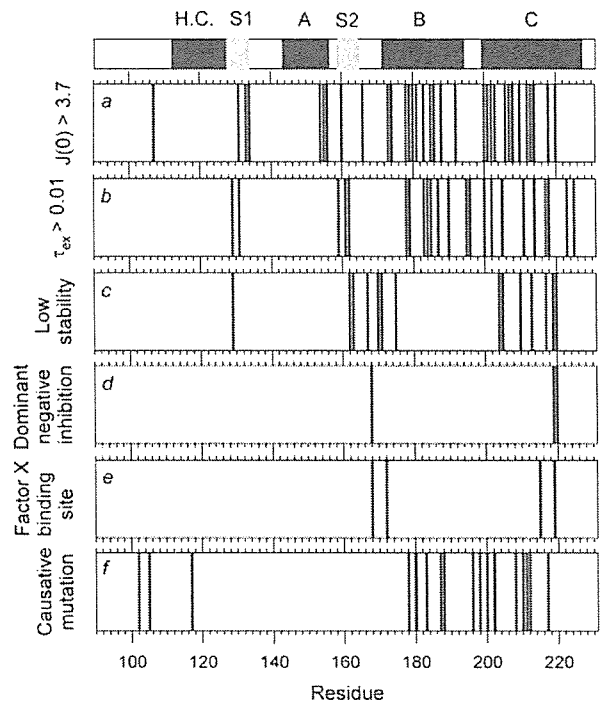

FIGURE 6: Plot of residues whose (a) $J(0)$ values are larger than 3.7 ns, obtained via reduced spectral density mapping, and (b) τ_{ex} values are larger than 0.01 s, obtained using the CPMG method. (c) Residues with low stability detected by high-pressure NMR. (d) Residues with polymorphisms exhibiting dominant negative inhibition of prion replication (*26*). (e) Residues mapped as the protein X binding epitope (*30*). (f) Residues whose mutations cause neurodegenerative diseases in humans.

We can speculate that conformational flexibility in the region facilitates factor X binding.

In PrP^C, slow fluctuations are evidently not connected to observed fast (picosecond-to-nanosecond) fluctuations. Amino acid residues predominantly fluctuating on the millisecond time scale mainly exist in helices B and C, which are also locally disordered in the PrP* intermediate state (*13*). This coincidence suggests that the slow dynamics of the prion protein includes trajectories from the native state to the thermodynamically distinct substate, PrP*. The thermodynamic picture derived from pressure-induced unfolding is not expected from the static NMR structure, nor from the dynamic picture on the picosecond-to-nanosecond time scale, which emphasizes the difference between unstructured N-terminal and structured C-terminal regions (*11*, *12*). Logically, millisecond time scale fluctuations may be qualitatively different from picosecond-to-nanosecond time scale motions (*31*−*33*). The overall coincidence between the stability and the slow dynamics suggests that the slow fluctuations of PrP occur along the reaction surface of the protein folding (*32*). However, the fast motions may just entail low energy fluctuations of the native structure. The curvature of the reaction surface for protein folding may not necessarily correspond to the local energy surface around the native PrP^C structure.

Correlations between Slow Fluctuations under Physiological Conditions and Pressure-Dependent Conformational Changes. The NMR relaxation analysis gives residue-specific amide chemical shift differences between two putative conformers that are considered to be mutually interconverting. These differences should reflect the amplitude of the conformational fluctuation at individual residue sites. On the other hand, from the relation between volume fluctuation and compressibility, pressure-induced chemical shift changes are also correlated with the amplitude of fluctuation at individual residues. As shown in Figure 5a, the chemical shift changes of amide ^{15}N nuclei induced by fluctuation, $\{f_1f_2\}^{1/2}\Delta\omega_{ex}$ with τ_{ex} larger than 1 ms, are correlated with the linear component of the pressure dependency of the ^{15}N chemical shift (*13*). This may suggest that slow fluctuations at ambient pressure are occurring within the basic folded subensemble (*34*). The basic folded subensemble is the "ensemble" of the native conformations with essentially the same compressibility exhibiting the linear pressure-dependent chemical shift changes. When they exhibit any nonlinear behavior, we presume it to be a transition from the basic folded structure to the low-lying excited state (*35*).

The amplitudes of the chemical shift fluctuations are about 10 times larger than those of the pressure-induced chemical shift changes. The average ^{15}N chemical shift difference between 1 and 2.5 kbar is ~0.1 ppm, which corresponds to a ψ angle of ~0.4° (*36*). On the other hand, the fluctuation of the ψ angle obtained by the CPMG relaxation experiment is ~4°, which is basically consistent with the results of many MD simulations (*37*). The Gibbs free energy of a protein is generally defined as a function of pressure (P) and temperature (T). In a thermal denaturation process under constant pressure, the entropic change ($T\Delta S$) is the main driving force, while in pressure denaturation at constant temperature, the volume change ($-P\Delta V$) is the major driving force. However, under approximately physiological conditions, a fluctuation may occur along a direction between them, as shown in Figure 7. The pressure-induced conformational changes emphasize the intermediate conformers with large ΔV, while temperature-induced conformational changes emphasize those with large ΔS. However, if a protein could fluctuate in a P/T plane freely during fluctuations, a small population may have a chance to reach a conformation with higher energy along the trajectories. This dynamic event may occur rarely, either because of the high energetic barrier (fast motion but with low probability) or by following a winding pathway along the rugged surface (slow motion). Either way, populat-

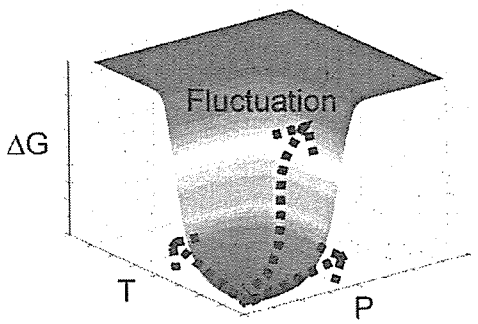

FIGURE 7: A sketch of the free energy landscape of a protein as a function of pressure (P) and temperature (T). Arrows on the right and left indicate the pressure and the temperature dependence, respectively, of the Gibbs free energy within the basic folded subensemble. The central arrow shows the effect of a fluctuation under physiological conditions occurring in a P/V plane.

ing the higher energy state occurs slowly.

Many intermediates in various proteins have been detected using high-pressure NMR (*34*). Why is pressure perturbation so sensitive for detecting intermediates compared to temperature perturbation? One reason may be that many intermediates are better defined in terms of volume than entropy. As long as protein folding occurs hierarchically with distinct volume changes, high-pressure NMR is quite useful to observe it. However, if an intermediate conformation has a volume similar to the native conformation, it may not be detected. Second, it must be noted that oligomers or aggregates, including amyloids, tend to dissociate into monomers under high pressure, while proteins generally tend to aggregate at high temperature. High-pressure NMR may prove advantageous for study of such intermolecular interactions.

CONCLUSIONS

Interaction between the C-terminal helical region and the hydrophobic cluster region of PrP^C was previously observed (*11*, *13*), and both regions are required for the infectivity (*38*). As noted, the pressure-induced collapse of cavities probably accounts for the observed NMR signal changes in helices B and C and in the S2-B loop and the β-strand S2. Because the hydrophobic cluster is also in contact with S2 and helix B (*11*), as shown in Figure 4, conformational transitions in this region can transduce a switch to possibly involve most of the structural elements identified in rPrP-(90−231) in promoting the $PrP^C \rightarrow PrP^{Sc}$ transformation. Pathogenicity itself must be directly related to the intermolecular interaction around the hydrophobic cluster regions, and the C-terminal helices may naturally prevent this intermolecular interaction. Modeling of PrP^{Sc} structure using electron microscopy has yielded models with intramolecular β-sheets while maintaining some helix structure (*39*). While progress on this difficult project is admirable, it is not possible at this stage to know with certainty whether the helices in PrP^{Sc} correspond precisely to those in PrP^C. PrP* presumably corresponds to an intermediate in the conversion process. Therefore, disease-causing mutations can increase the population of PrP*, which enables access to the hydrophobic cluster via the local conformational disorder of helices B and C. This may promote the conformational conversion process by intermolecular interaction at the hydrophobic cluster, resulting in the intermolecular β-sheet formation characteristic of PrP^{Sc}.

SUPPORTING INFORMATION AVAILABLE

Representative examples of the nonlinear curve fits of the relaxation dispersion data. This information is available free of charge via the Internet at http://pubs.acs.org.

REFERENCES

1. Chazot, G., Broussolle, E., Lapras, C. I., Blättler, T., Aguzzi, A., and Kopp, N. (1996) New Variant of Creutzfeldt-Jakob Disease in a 26-Year-Old French Man. *Lancet 347*, 1181.
2. Will, R. G., Ironside, J. W., Zeidler, M., Cousens, S. N., Estibeiro, K., Alperovitch, A., Poser, S., Pocchiari, M., Hofman, A., and Smith, P. G. (1996) A New Variant of Creutzfeldt-Jakob Disease in the UK. *Lancet. 347*, 921−925.
3. Prusiner, S. B. (1982) Novel proteinaceous infectious particles cause scrapie. *Science 216*, 136−144.
4. Prusiner, S. B. (1991) Molecular Biology of Prion Diseases. *Science 252*, 1515−1522.
5. Stahl, N., Baldwin, M. A., Teplow, D. B., Hood, L., Gibson, B. W., Burlingame, A. L., and Prusiner, S. B. (1993) Structural studies of the scrapie prion protein using mass spectrometry and amino acid sequencing. *Biochemistry 32*, 1991−2002.
6. Pan, K.-M., Baldwin, M., Nguyen, J., Gasset, M., Serban, A., Groth, D., Mehlhorn, I., Huang, Z., Fletterick, R. J., Cohen, F. E., and Prusiner, S. B. (1993) Conversion of α-Helices into β-Sheets Features in the Formation of the Scrapie Prion Proteins. *Proc. Natl. Acad. Sci. U.S.A. 90*, 10962−10966.
7. Riek, R., Hornemann, S., Wider, G., Billeter, M., Glockshuber, R., and Wüthrich, K. (1996) NMR Structure of the Mouse Prion Protein Domain PrP(121−231). *Nature 382*, 180−182.
8. James, T. L., Liu, H., Ulyanov, N. B., Farr-Jones, S., Zhang, H., Donne, D. G., Kaneko, K., Groth, D., Mehlhorn, I., Prusiner, S. B., and Cohen, F. E. (1997) Solution structure of a 142-residue recombinant prion protein corresponding to the infectious fragment of the scrapieisoform. *Proc. Natl. Acad. Sci. U.S.A. 94*, 10086−10091.
9. Lopez Garcia, F., Zahn, R., Riek, R., and Wuthrich, K. (2000) NMR structure of the bovine prion protein. *Proc. Natl. Acad. Sci. U.S.A. 97*, 8334−8339.
10. Calzolai, L., Lysek, D. A., Guntert, P., von Schroetter, C., Riek, R., Zahn, R., and Wuthrich, K. (2000) NMR structures of three single-residue variants of the human prion protein. *Proc. Natl. Acad. Sci. U.S.A. 97*, 8340−8345.
11. Liu, H., Farr-Jones, S., Ulyanov, N. B., Llinas, M., Marqusee, S., Groth, D., Cohen, F. E., Prusiner, S. B., and James, T. L. (1999) Solution structure of Syrian hamster prion protein rPrP(90−231). *Biochemistry 38*, 5362−5377.
12. Viles, J. H., Donne, D., Kroon, G., Prusiner, S. B., Cohen, F. E., Dyson, H. J., and Wright, P. E. (2001) Local structural plasticity of the prion protein. Analysis of NMR relaxation dynamics. *Biochemistry 40*, 2743−2753.
13. Kuwata, K., Li, H., Yamada, H., Legname, G., Prusiner, S. B., Akasaka, K., and James, T. L. (2002) Locally disordered conformer of the hamster prion protein: a crucial intermediate to PrP^{Sc}? *Biochemistry 41*, 12277−12283.
14. Luz, Z., and Meiboom, S. (1963) Nuclear Magnetic Resonance Study of the Protolysis of Trimethylammonium Ion in Aqueous Solution − Order of the Reaction with Respect to Solvent. *J. Chem. Phys. 39*, 366.
15. Prusiner, S. B. (1996) Human Prion Diseases and Neurodegeneration. *Curr. Top. Microbiol. Immunol. 207*, 1−17.
16. Buevich, A. V., and Baum, J. (1999) Dynamics of unfolded proteins: incorporation of distributions of correlation times in the model free analysis of NMR relaxation data. *J. Am. Chem. Soc. 121*, 8671−8672.
17. Uversky, V. N. (2002) Natively unfolded proteins: a point where biology waits for physics. *Protein Sci. 11*, 739−756.
18. Farrow, N. A., Zhang, O., Forman-Kay, J. D., and Kay, L. E. (1995) Comparison of the backbone dynamics of a folded and an unfolded SH3 domain existing in equilibrium in aqueous buffer. *Biochemistry 34*, 868−878.

19. Mulder, F. A. A., Spronk, C. A., E. M., Slijper, M., Kaptein, R., and Boelens, R. (1996) Improved HSQC Experiments for the Observation of Exchange Broadened Signals. *J. Biomolec. NMR. 8*, 223−228.
20. van Tilborg, P. J., Mulder, F. A., de Backer, M. M., Nair, M., van Heerde, E. C., Folkers, G., van der Saag, P. T., Karimi-Nejad, Y., Boelens, R., and Kaptein, R. (1999) Millisecond to microsecond time scale dynamics of the retinoid X and retinoic acid receptor DNA-binding domains and dimeric complex formation. *Biochemistry 38*, 1951−1956.
21. Palmer, A. G., III, Skelton, N. J., Chazin, W. J., Wright, P. E., and Rance, M. (1992) Suppression of the effects of cross-correlation between dipolar and anisotropic chemical shift relaxation mechanisms in the measurement of spin spin relaxation rates. *Mol. Phys. 75*, 699−711.
22. Millet, O., Loria, J. P., Kroenke, C. D., Pons, M., and Palmer, A. G., 3rd. (2000) The Static Magnetic Field Dependence of Chemical Exchange Linebroadening Defines the NMR Chemical Shift Time Scale. *J. Am. Chem. Soc. 122*, 2867−2877.
23. Davis, D. G., Perlman, M. E., and London, R. E. (1994) Direct measurements of the dissociation rate constant for inhibitor-enzyme complexes via the T1 rho and T2 (CPMG) methods. *J. Magn. Reson. B. 104*, 266−275.
24. Shmerling, D., Hegyi, I., Fischer, M., Blättler, T., Brandner, S., Götz, J., Rülicke, T., Flechsig, E., Cozzio, A., von Mering, C., Hangartner, C., Aguzzi, A., and Weissmann, W. (1998) Expression of Amino-Terminally Truncated PrP in the Mouse Leading to Ataxia and Specific Cerebellar Lesions. *Cell 93*, 203−214.
25. Muramoto, T., DeArmond, S. J., Scott, M., Telling, G. C., Cohen, F. E., and Prusiner, S. B. (1997) Heritable disorder resembling neuronal storage disease in mice expressing prion protein with deletion of an alpha-helix. *Nat. Med. 3*, 750−755.
26. Perrier, V., Kaneko, K., Safar, J., Vergara, J., Tremblay, P., DeArmond, S. J., Cohen, F. E., Prusiner, S. B., and Wallace, A. C. (2002) Dominant-negative inhibition of prion replication in transgenic mice. *Proc. Natl. Acad. Sci. U.S.A. 99*, 13079−13084.
27. Zhang, H., Stöckel, J., Mehlhorn, I., Groth, D., Baldwin, M. A., Prusiner, S. B., James, T. L., and Cohen, F. E. (1997) Physical Studies of Conformational Plasticity in a Recombinant Prion Protein. *Biochemistry 36*, 3543−3553.
28. Hornemann, S., and Glockshuber, R. (1998) A scrapie-like unfolding intermediate of the prion protein domain PrP(121−231) induced by acidic pH. *Proc. Nat. Acad. Sci. U.S.A. 95*, 6010−6014.
29. Apetri, A. C., and Surewicz, W. K. (2002) Kinetic intermediate in the folding of human prion protein. *J. Biol. Chem. 277*, 44589−44592.
30. Kaneko, K., Zulianello, L., Scott, M., Cooper, C. M., Wallace, A. C., James, T. L., Cohen, F. E., and Prusiner, S. B. (1997) Evidence for protein X binding to a discontinuous epitope on thecellular prion protein during scrapie prion propagation. *Proc. Natl. Acad. Sci. U.S.A. 94*, 10069−10074.
31. Garcia, A. E., and Hummer, G. (1999) Conformational dynamics of cytochrome *c*: correlation to hydrogen exchange. *Proteins 36*, 175−191.
32. Karplus, M. (2000) Aspects of protein reaction dynamics: deviations from simple behavior. *J. Phys. Chem. B. 104*, 11−27.
33. Komatsuzaki, T., and Berry, R. S. (2001) Dynamical hierarchy in transition states: why and how does a system climb over the mountain? *Proc. Natl. Acad. Sci. U.S.A. 98*, 7666−7671.
34. Akasaka, K. (2003) Highly fluctuating protein structures revealed by variable-pressure nuclear magnetic resonance. *Biochemistry 42*, 10875−10885.
35. Akasaka, K., and Li, H. (2001) Low-lying excited states of proteins revealed from nonlinear pressure shifts in ^{1}H and ^{15}N NMR. *Biochemistry 40*, 8665−8671.
36. Akasaka, K., Li, H., Yamada, H., Li, R. H., Thoresen, T., and Woodward, C. K. (1999) Pressure response of protein backbone structure. Pressure-induced amide ^{15}N chemical shifts in BPTI. *Protein Sci. 8*, 1946−1953.
37. Tai, K., Shen, T., Borjesson, U., Philippopoulos, M., and McCammon, J. A. (2001) Analysis of a 10-ns molecular dynamics simulation of mouse acetylcholinesterase. *Biophys. J. 81*, 715−724.
38. Muramoto, T., Scott, M., Cohen, F., and Prusiner, S. B. (1996) Recombinant scrapie-like prion protein of 106 amino acids is soluble. *Proc. Natl. Acad. Sci. U.S.A. 93*, 15457−15462.
39. Wille, H., Michelitsch, M. D., Guenebaut, V., Supattapone, S., Serban, A., Cohen, F. E., Agard, D. A., and Prusiner, S. B. (2002) Structural studies of the scrapie prion protein by electron crystallography. *Proc. Nat. Acad. Sci. U.S.A. 99*, 3563−3568.

BI036123O

Available online at www.sciencedirect.com
SCIENCE DIRECT®
Biochemical and Biophysical Research Communications 319 (2004) 50–57
BBRC
www.elsevier.com/locate/ybbrc

RNAi induction and activation in mammalian muscle cells where *Dicer* and *eIF2C* translation initiation factors are barely expressed

Noriko Sago,[a,b,1] Kazuya Omi,[a,b,1] Yoshiko Tamura,[a] Hiroshi Kunugi,[a] Teruhiko Toyo-oka,[c] Katsushi Tokunaga,[b] and Hirohiko Hohjoh[a,*]

[a] *National Institute of Neuroscience, NCNP, 4-1-1 Ogawahigashi, Kodaira, Tokyo 187-8502, Japan*
[b] *Department of Human Genetics, Graduate School of Medicine, The University of Tokyo, 7-3-1 Hongo, Bunkyo-ku, Tokyo 113-0033, Japan*
[c] *Department of Pathophysiology and Internal Medicine, The University of Tokyo, 7-3-1 Hongo, Bunkyo-ku, Tokyo 113-0033, Japan*

Received 25 February 2004
Available online 10 May 2004

Abstract

Dicer plays an important role in the course of RNA interference (RNAi), i.e., it digests long double-stranded RNAs into 21–25 nucleotide small-interfering RNA (siRNA) duplexes functioning as sequence-specific RNAi mediators. In this study, we investigated the expression levels of *Dicer* and *eIF2C1~4*, which, like *Dicer*, appear to participate in mammalian RNAi, in various mouse tissues. Results indicate that the levels of *eIF2C1~4* as well as *Dicer* are lower in skeletal muscle and heart than in other tissues. To see if RNAi could occur under such a condition with low levels of expression of *Dicer* and *eIF2C1~4*, we examined RNAi activity in mouse skeletal muscle fibers. The results indicate that RNAi can be induced by synthetic siRNA duplexes in muscle fibers. We further examined RNAi activity during myogenic differentiation of mouse C2C12 cells. The data indicate that although the expression levels of *Dicer* and *eIF2C1~4* decrease during the differentiation, RNAi can be induced in the cells. Altogether, the data presented here suggest that muscle cells retain the ability to induce RNAi, although *Dicer* and *eIF2C1~4* appear to be barely expressed in them.

Keywords: RNA interference; Dicer; eIF2C translation initiation factors; Muscle; C2C12 cell

RNA interference (RNAi) is the process of a sequence-specific post-transcriptional gene silencing triggered by double-stranded RNAs (dsRNAs) homologous to the silenced genes. This intriguing gene silencing has been found in various species including flies, worms, protozoa, vertebrates, and higher plants (reviewed in [1–4]). DsRNAs introduced or generated in cells are digested by an RNase III enzyme, Dicer, into 21–25 nucleotide (nt) RNA duplexes [5–8] and the resultant duplexes, referred to as small-interfering RNA (siRNA) duplexes, function as essential sequence-specific RNAi mediators in the RNA-induced silencing complexes (RISCs) [5,7]. Thus, Dicer appears to play an important role in the process of RNAi induction.

In mammalian cells except for a part of undifferentiated cells [9–12], long dsRNAs (>30 bp) can trigger a rapid and non-specific RNA degradation involving the sequence-non-specific RNase, RNase L [13], and a rapid translation inhibition involving the interferon-inducible, dsRNA-activated protein kinase, PKR, instead of induction of RNAi [14]. In contrast, chemically synthesised siRNA duplexes can induce the sequence-specific RNAi activity in mammalian cells without triggering the rapid and non-specific RNA degradation and translation inhibition [15]. Together, it is likely that RNAi activity induced by the long dsRNAs could be masked by those rapid responses to the long dsRNAs in most of mammalian cells.

It may be of interest to examine the role of Dicer in differentiated mammalian cells possessing the rapid responses to long dsRNAs. Mammalian dicer has been identified and found to be a large multi-domain

* Corresponding author. Fax: +81-42-346-1744.
E-mail address: hohjohh@ncnp.go.jp (H. Hohjoh).
[1] These authors contributed equally to this work.

0006-291X/$ - see front matter © 2004 Elsevier Inc. All rights reserved.
doi:10.1016/j.bbrc.2004.04.151

polypeptide (~215 kDa) characterised by containing a putative DExH/DEAH RNA helicase/ATPase domain, a PAZ domain, two RNase domains, and a dsRNA-binding domain [16–20]. The expression of *Dicer* appears to be ubiquitous, but the level of its expression varies among tissues. Of the tissues examined previously, skeletal muscle appeared to express *Dicer* at a low level, i.e., the *Dicer* transcript appeared to be barely detectable at least using RT-PCR [16,17].

In this study, we investigated not only RNAi activity but also the expression levels of *Dicer* and *eIF2C1~4*, which, like *Dicer*, appear to participate in mammalian RNAi [21,22], in mouse skeletal muscle fibers, and muscle cells that differentiated from mouse C2C12 cells. The results indicate that RNAi can be induced by synthetic siRNA duplexes in those cells although the expression levels of *Dicer* and *eIF2C1~4* are lower than those in other tissues and undifferentiated C2C12 cells.

Materials and methods

Preparation and culture of muscle fibers isolated from extensor digitorum longus in mice. Isolation of muscle fibers from mice was carried out as described previously [23]. Briefly, extensor digitorum longus (EDL) was isolated from mice (ICR mouse strain), treated with 0.5% type 1 collagenase (Washington biochemical) in Dulbecco's modified Eagle's medium (DMEM) (Sigma), and incubated at 37 °C for 90 min. After incubation, the EDL was dissociated into single muscle fibers by gently pipetting, and dissociated single fibers were plated on matrigel-coated 24-well culture plates (approximately 100 fibers/well). The muscle fibers were cultured at 37 °C in DMEM supplemented with 10% horse serum (Invitrogen) in a 5% CO_2-humidified chamber. Two–three hours after starting culture, transfection was carried out.

Cell culture. C2C12 cells were grown at 37 °C in DMEM supplemented with 15% fetal calf serum (Sigma), 100 U/ml penicillin (Invitrogen), and 100 μg/ml streptomycin (Invitrogen) in a 5% CO_2-humidified chamber. For induction of myogenic differentiation, cells were cultured at 37 °C in DMEM supplemented with 5% horse serum (Invitrogen) in a 5% CO_2-humidified chamber [24]. The medium was changed everyday.

Synthetic oligonucleotides. RNA and DNA synthetic oligonucleotides were obtained from PROLIGO and SIGMAGENOSIS, respectively. The La2 siRNA duplex described previously was used in this study, and preparation of RNA duplexes was performed as described previously [25].

Transfection and luciferase assay. Reporter plasmids and siRNA duplexes were cotransfected into isolated single muscle fibers and undifferentiated and differentiated C2C12 cells using Lipofectamine 2000 (Invitrogen) according to the manufacturers' instructions. When undifferentiated C2C12 cells were used, the day before transfection, the cells were trypsinised, diluted with the fresh medium without

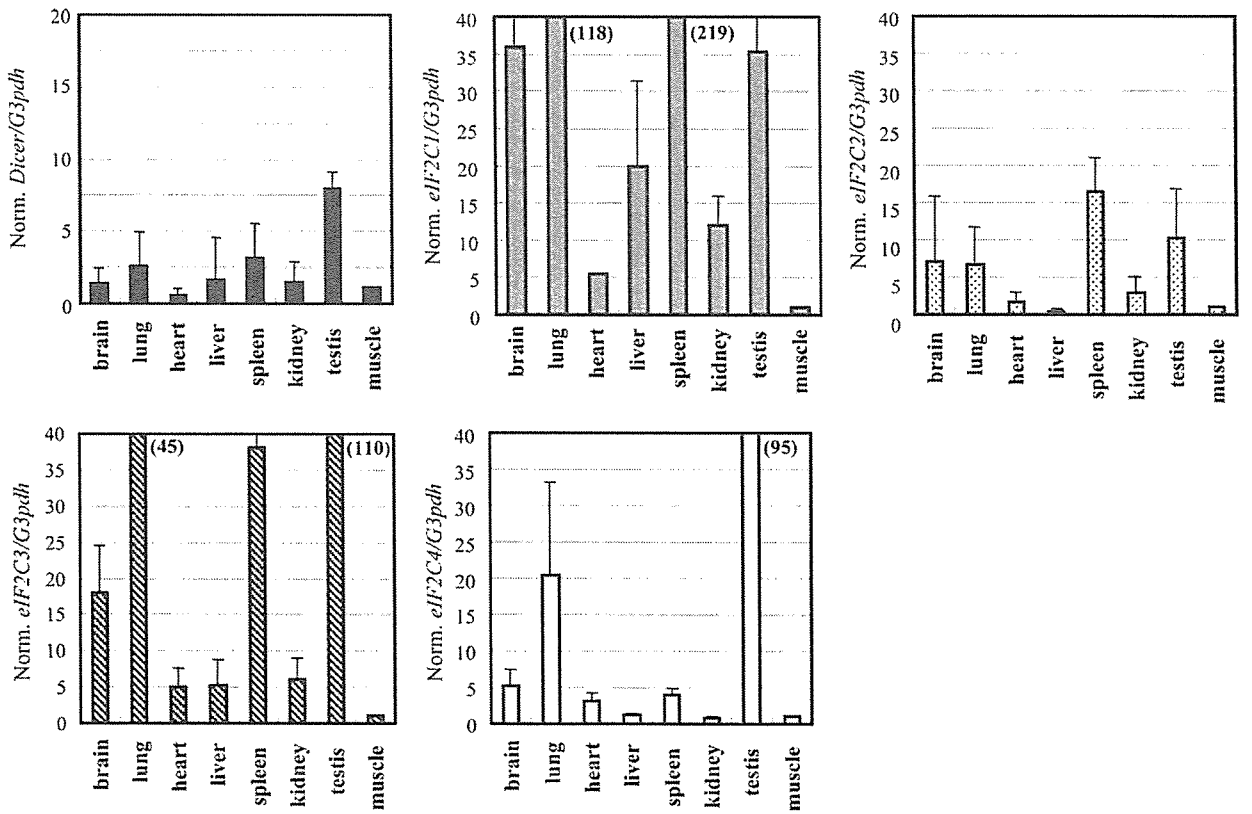

Fig. 1. Expression profiles of *Dicer* and *eIF2C1~4* in various mouse tissues. Total RNA was extracted from indicated tissues and subjected to cDNA synthesis with oligo(dT) primer and a reverse transcriptase. The expression levels of *Dicer* and *eIF2C1~4* were examined by means of a real-time PCR using the synthesised cDNAs as templates. The expression levels of the genes are normalised to that of the *G3pdh* gene examined as a control, and plotted when the expression level of either *Dicer* or *eIF2C1~4* in skeletal muscle is given as 1. Figures in parentheses indicate the averaged expression levels which are over the plotted areas. Data are averages of three independent experiments. Error bars represent standard deviations.

antibiotics, and seeded into 24-well culture plates (approximately 5×10^4 cells/well). Before the transfection, the culture medium was replaced with 0.5 ml OPTI-MEM I (Invitrogen), and to each well, 0.25 μg pGL3-control plasmid (Promega), 0.05 μg pRL-SV40 plasmid (Promega), and 0.2 μg siRNAs were applied. After 4-h incubation, 0.5 ml of the fresh culture medium without antibiotics was added, and further incubation at 37 °C was carried out. In the case of transfection into the isolated muscle fibers, the transfection mixture was directly applied into wells, and further incubation at 37 °C was carried out. When a short-hairpin expression plasmid, pRNA-U6.1/Neo/siRNA (GenScript), was used instead of synthetic siRNAs, 0.1 μg pGL3-control and 0.05 μg phRL-TK (Promega) together with various amounts of pRNA-U6.1/Neo/siRNA were introduced into C2C12 cells. The expression of luciferase was examined using a Dual-Luciferase reporter assay system (Promega) according to the directions provided by the manufacturer.

RT-PCR. Total RNA was extracted from the cultured cells and various mouse tissues using Trizol reagent (Invitrogen). Reverse-transcription (RT) for synthesizing the first-strand cDNAs was carried out using oligo(dT) primer and SuperScript II reverse transcriptase (Invitrogen) according to the manufacturer's instructions, and the resultant cDNAs were examined by real-time PCR using the ABI PRISM 7000 sequence detection system (Applied Biosystems) with a SYBER Green PCR Master Mix or a TaqMan Universal PCR Master Mix together with Assays-on-Demand Gene Expression products (Applied Biosystems) according to the manufacturer's instructions. For plotting a standard curve, the 1, 5, 25, 125, and 625-fold diluted brain cDNA samples, which were prepared from a brain tissue (total RNA) and designated as standards, were used in every real-time PCR. Expression levels of the genes examined were normalised to that of the control *G3pdh* gene. The PCR primers used in the real-time PCR were as follows:

G3pdh-F; 5′-TCTTCACCACCATGGAGAAG-3′
G3pdh-R; 5′-TCATGGATGACCTTGGCCAG-3′
Dicer-F; 5′-GCAGGCTTTTACACACGCCT-3′
Dicer-R; 5′-GGGTCTTCATAAAGGTGCTT-3′
eIF2C2-F; 5′-AGATGAAGAGGAAGTACCGT-3′
eIF2C2-R; 5′-CAGAACCAGCTTGTGCCTGT-3′

The Assays-on-Demand Gene Expression products used (the Assay ID numbers) were as follows:

eIF2C1; Mm00462977m1, *eIF2C3*; Mm00462959m1, *eIF2C4*; Mm00462659m1.

5-Bromodeoxyuridine incorporation assay. Cells were metabolically labeled in the culture medium containing 10 μM of 5-bromodeoxyuridine (BrdU) (Sigma) for 20 h, and rinsed with phosphate-buffered saline solution (PBS) followed by fixation with 70% ethanol containing 0.5 M HCl at −20 °C for 1 h. The resultant cells were incubated with anti-BrdU antibody (Oxford biotechnology) at 4 °C overnight. The BrdU-antibody complexes were visualised with Alexa488 conjugated secondary antibody (Invitrogen) and examined using a ZEISS (Axiovert) microscope.

Results and discussion

Expression profiles of Dicer and eIF2C1~4 in various mouse tissues

Previous studies suggested that *Dicer* and *eIF2C* translation initiation factors (*eIF2C1~4*) homologous to the *Ago* genes in *Drosophila* [26,27] contributed to mammalian RNAi [21,22]. *Dicer* appears to be expressed ubiquitously, but its expression level varies among tissues [16,17]. Since little is known about the expression levels of *eIF2C1~4* among tissues, we first examined the levels of expression of *eIF2C1~4* and *Dicer* in various tissues. Total RNA was extracted from mouse tissues and subjected to cDNA synthesis with oligo(dT) primer and reverse transcriptase. The resultant cDNAs were examined by a real-time PCR. The results are shown in Fig. 1. The expression level of *Dicer* in either skeletal muscle or heart appears to be lower than those in other tissues, which agrees with the previous observations [16,17]. It should be noted that the expression levels of *eIF2C1~4* in either skeletal muscle or heart, like the expression profile of *Dicer*, are also significantly lower than those in the other tissues examined. Consequently, the observations suggest that

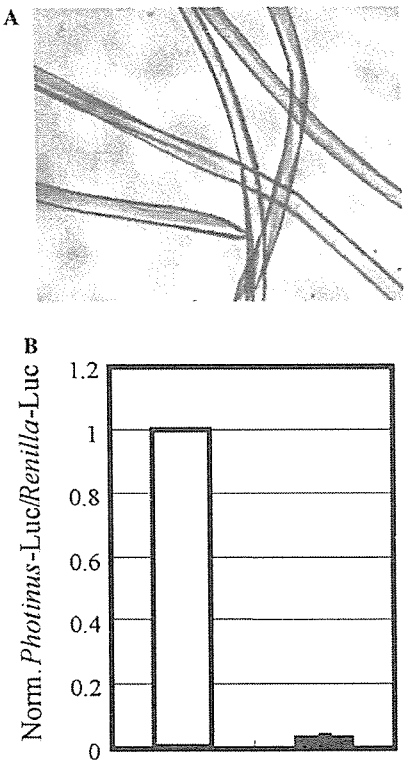

Fig. 2. RNAi induction by synthetic siRNA duplexes in muscle fibers prepared from mouse extensor digitorum longus. (A) Photograph of isolated muscle fibers. Isolation of muscle fibers from mouse extensor digitorum longus was carried out as described in Materials and methods. (B) RNAi activity in isolated muscle fibers. The La2 siRNA duplex against the *Photinus* luciferase gene [25] or a non-silencing siRNA duplex (Qiagen) together with pGL3-control and pRL-SV40 plasmids carrying *Photinus* and *Renilla* luciferase reporter genes, respectively, were cotransfected into the isolated muscle fibers. Twenty-four hours after transfection, cell lysate was prepared and dual luciferase assay was carried out. Ratios of normalised target (*Photinus*) luciferase activity to control (*Renilla*) luciferase activity are indicated: the ratios of luciferase activity determined in the presence of the La2 siRNA duplex are normalised to the ratios obtained in the presence of the non-silencing siRNA duplex. Open and solid bars indicate the data in the presence of the non-silencing siRNA and La2 siRNA duplexes, respectively. Data are averages of at least three independent experiments. Error bars represent standard deviations.

skeletal and cardiac muscle cells express either *Dicer* or *eIF2C1~4* at a low level.

RNAi activity in muscle fibers isolated from mouse extensor digitorum longus

The observations described above raised the question whether RNAi could occur in muscle, i.e., whether RNAi could be induced under a condition with a low level of expression of either *Dicer* or *eIF2C1~4*. In order to address the question, we isolated mouse muscle fibers from extensor digitorum longus of ICR mice (Fig. 2A), and introduced synthetic 21-nt siRNA duplex targeting the exogenous reporter gene, *Photinus* luciferase, together with a pGL3-control plasmid carrying the *Photinus luciferase* gene and a pRL-SV40 plasmid carrying the *Renilla luciferase* gene as a control into the isolated muscle fibers. For realizing an efficient RNAi induction, we used the La2 siRNA duplex having the potential for inducing a strong RNAi activity in cultured mammalian cells [25]. As shown in Fig. 2B, the results indicate that the La2 siRNA duplex can induce a strong gene silencing of the *Photinus luciferase* gene in the muscle fibers. This result suggests that RNAi can be induced by synthetic siRNA duplexes in skeletal muscle which barely expresses either *Dicer* or *eIF2C1~4*.

RNAi activity during myogenic differentiation of mouse C2C12 cells

To further examine the properties of RNAi in muscle cells and during myogenic differentiation, we investigated RNAi activity in C2C12 cells, a mouse myoblast cell line, which can be induced by changing culture conditions (detailed in Materials and methods) to differentiate into contractile myotubes [24]. First, we

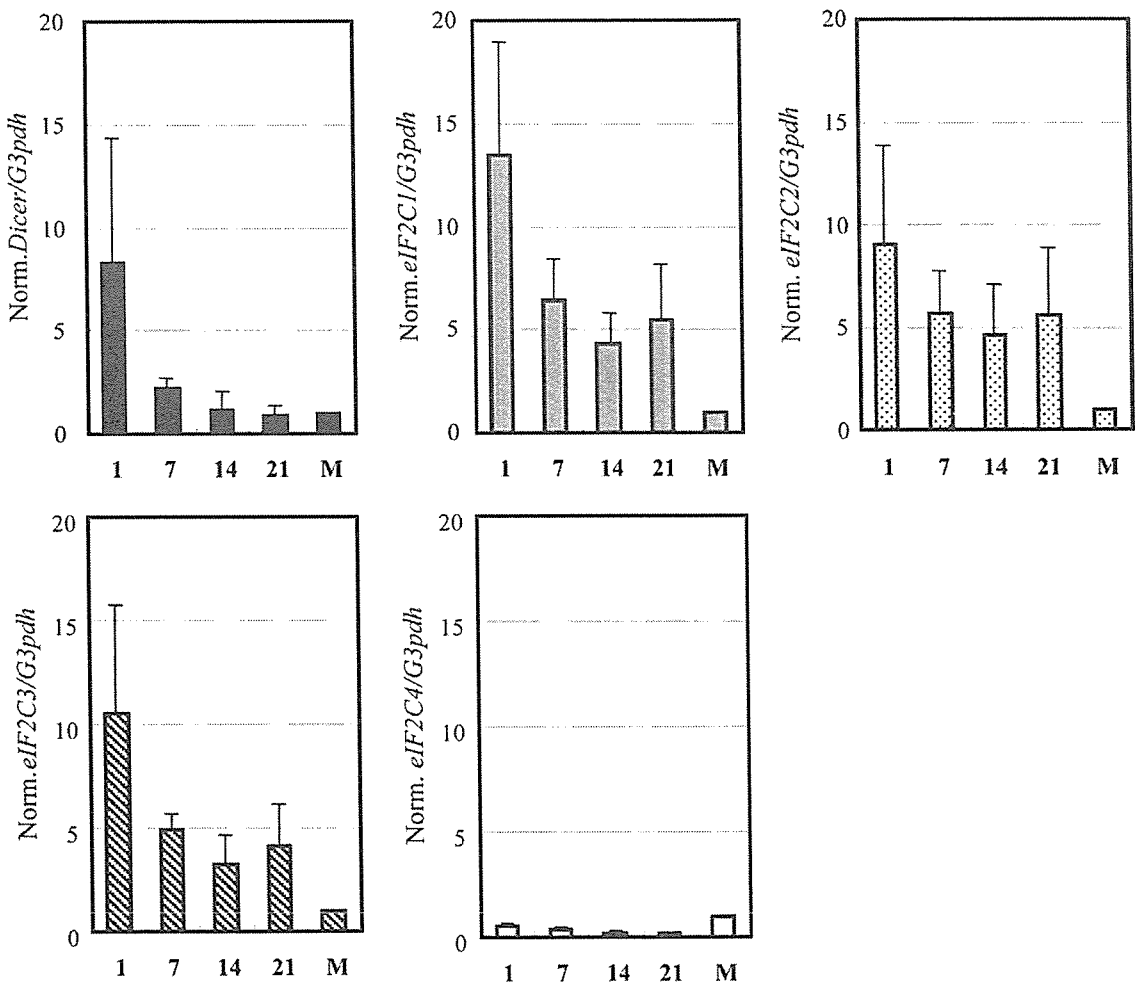

Fig. 3. Expression profiles of *Dicer* and *eIF2C1~4* during myogenic differentiation of mouse C2C12 cells. Total RNA was extracted from C2C12 cells at various days (indicated) after induction of myogenic differentiation of the cells (day 1 indicates undifferentiated C2C12 cells), and subjected to RT-PCR to examine the expression levels of *Dicer* and *eIF2C1~4* as in Fig. 1. The expression levels of the genes are normalised and plotted as in Fig. 1. M indicates skeletal muscle. Data are averages of three independent experiments. Error bars represent standard deviations.